JCB Journal of Cell Biology

ARTICLE

The Unkempt RNA-binding protein reveals a local translation program in centriole overduplication

Abraham Martinez[1], Alexander J. Stemm-Wolf[1], Ryan M. Sheridan[2], J. Matthew Taliaferro[2,3], and Chad G. Pearson[1]

Excess centrosomes cause defects in mitosis, cell-signaling, and cell migration, and therefore their assembly is tightly regulated. The divergent Polo kinase, PLK4, controls centriole duplication at the heart of centrosome assembly, and elevated PLK4 levels promote centrosome amplification (CA), a founding event of tumorigenesis. Here, we investigate the transcriptional consequences of elevated PLK4 and find *Unkempt* (UNK), a gene encoding an RNA-binding protein with roles in mRNA translational regulation, to be one of only two upregulated mRNAs. UNK protein localizes around centrosomes and with CEP131-positive centriolar satellites, promoting CEP131 localization to and around centrosomes. UNK's RNA-binding activity is required for PLK4-induced centriole overduplication. Consistent with the loss in PLK4-induced centriole overduplication, UNK depletion disrupts PLK4 and centriole assembly protein localization. Finally, translation is enriched at centrosomes and centriolar satellites, with UNK and CEP131 promoting this localized translation. In summary, UNK and CEP131 promote PLK4 localization and local translation at centrosomes during centriole overduplication.

Introduction

Centrosomes, composed of a pair of centrioles and pericentriolar material, nucleate and organize the microtubules (MTs) of the mitotic spindle during cell division. During interphase, centrosomes, along with the Golgi apparatus, nucleate MTs for general endo-lysosomal transport and for the transport of cargoes to and from the centrosome (Naslavsky and Caplan, 2020). At G1 of the cell cycle, a single centrosome is present in each cell. A second centrosome is assembled during S phase, and this is controlled primarily by the Polo-like kinase, PLK4, which phosphorylates and recruits proteins to the site of nascent centriole assembly (Moyer and Holland, 2019; Kleylein-Sohn et al., 2007). Like DNA replication, centriole assembly is tightly regulated to once and only once each cell cycle (Nigg and Holland, 2018). The dysregulation of centriole assembly proteins can lead to centriole overduplication and centrosome amplification (CA). Consequences of CA include multipolar mitoses, cell death, aneuploidy, chromosome missegregation, and chromosome instability (Coelho et al., 2015; Denu et al., 2018; Ganapathi Sankaran et al., 2019; Zhou et al., 1998; Pihan et al., 1998; Ghadimi et al., 2000). These abnormalities result in human diseases, including microcephaly (Marthiens et al., 2013) and cancer (Levine et al., 2017).

Centriole duplication begins at the G1 to S phase transition, where PLK4 is recruited to the two centrioles of the centrosome. PLK4 associates with the centrioles through its interactions with the centriole wall complex proteins, CEP63–CEP152 and CEP192–CEP152 (Brown et al., 2013; Sonnen et al., 2013). PLK4 coalesces at the site of daughter procentriole formation (Ohta et al., 2014). PLK4 phosphorylates STIL and promotes the recruitment of additional centriole proteins required for centriole assembly (Ohta et al., 2014; Moyer and Holland, 2019; Dzhindzhev et al., 2017). Following daughter centriole assembly, the two centrosomes comprising four centrioles mature through the cell cycle. Because the protein level and centrosome localization of PLK4 can dictate how many centrioles will form (Moyer and Holland, 2019), PLK4 is tightly regulated to prevent promiscuous centriole assembly (Čajánek et al., 2015; Cunha-Ferreira et al., 2013; Rogers et al., 2009). An increase in the levels of PLK4 at centrioles promotes centriole overduplication and results in CA (Coelho et al., 2015). To prevent this, PLK4 autophosphorylation promotes its own degradation in a ubiquitin-mediated proteosome-dependent manner (Cunha-Ferreira et al., 2013; Klebba et al., 2013). Therefore, controlled centriole duplication and assembly require that centriole proteins cooperate to regulate the stability of PLK4 and its specific localization at mother centrioles.

PLK4 also has a role in regulating its own stability at the centrioles through its effect on centriolar satellite proteins (Kim et al., 2019). Centriolar satellites are membraneless, electron-dense granules that scaffold and transport cargoes to and from

[1]Department of Cell and Developmental Biology, University of Colorado, Anschutz Medical Campus, Aurora, CO, USA; [2]RNA Bioscience Initiative (RBI), University of Colorado, Anschutz Medical Campus, Aurora, CO, USA; [3]Department of Biochemistry and Molecular Genetics, University of Colorado, Anschutz Medical Campus, Aurora, CO, USA.

Correspondence to Chad G. Pearson: chad.pearson@cuanschutz.edu.

the centrosome in an MT-dependent manner (Conkar et al., 2019; Staples et al., 2012; Stemm-Wolf et al., 2021). Cargoes include centrosome assembly proteins, ubiquitylating and deubiquitylating proteins, and components involved in ciliogenesis (Aydin et al., 2020; Kubo et al., 1999; Gheiratmand et al., 2019; Gupta et al., 2015). PLK4 phosphorylates the major scaffolding centriolar satellite proteins CEP131 and PCM1 to maintain their centrosome localization, which in turn stabilizes PLK4 at centrioles (Kim et al., 2019). Therefore, in addition to PLK4 regulating its own stability through autophosphorylation, PLK4 modulates trafficking structures to promote stabilized PLK4 complexes at centrioles.

Our current understanding of centriole duplication is limited to protein–protein interactions and the recruitment and transport to the centrosome of centriole assembly proteins that cooperate with PLK4. mRNAs encoding centriole and centrosome proteins localize to centrosomes for local translation and centrosome regulation (Lerit, 2022). How RNAs are trafficked and the mechanisms by which translation is regulated at centrosomes are poorly understood. Local translation at centrosomes has been primarily studied in mitosis (Safieddine et al., 2021), so whether local translation occurs at centrosomes to regulate centriole duplication is unknown. In support of this possibility, RNAs have been localized to the centrosome during interphase when centriole duplication and centrosome maturation occur (Safieddine et al., 2021). Moreover, RNA-binding proteins (RBPs) localize to centrosomes (Filippova et al., 2012; Jao et al., 2017; Ishigaki et al., 2014). Intriguingly, proteomics studies identifying interactions with centrosome and centriolar satellite proteins have found multiple RBPs, translation elongation and initiation factors, ribosomal proteins, and other RNA-processing machinery (Gheiratmand et al., 2019; Gupta et al., 2015; Arslanhan et al., 2020). This suggests that centriolar satellites may regulate centrosome-associated translation. Whether centriolar satellites are involved in the trafficking of RNAs, local translation, or other RNA regulatory processes concomitant with cell cycle–dependent centrosome functions such as centriole duplication is unknown (Kubo et al., 1999; Dammermann and Merdes, 2002). Because PLK4 phosphorylates centriolar satellite proteins, in addition to other centriole and centrosome proteins to regulate their localization and cargo transport to centrosomes, centriolar satellite regulation may also be required to deliver translational machinery, RNAs, or RNA-processing complexes necessary for centriole duplication (Denu et al., 2019; Moyer and Holland, 2019; Ohta et al., 2014; Hori et al., 2016; Lee et al., 2017; Bergalet et al., 2020; Sepulveda et al., 2018).

We identified the RBP, *Unkempt* (UNK) gene, to be upregulated when PLK4 levels are elevated. UNK localizes around centrosomes and with centriolar satellites, and its RNA-binding activity is necessary for PLK4-induced centriole overduplication. UNK depletion decreases the amounts of centriole assembly proteins at centrosomes and results in the dispersal of the centriolar satellite proteins CEP131 and PCM1. Like UNK, CEP131 promotes PLK4-induced centriole overduplication. We identify centriolar satellites as sites of active translation and find that UNK and CEP131 promote the localization of nascent proteins at centrosomes. In summary, UNK promotes the localization of centriole assembly proteins, centriolar satellites, translation at centrosomes, and facilitates PLK4-induced centriole overduplication.

Results

The UNK RBP facilitates PLK4-induced centriole overduplication

PLK4 levels are commonly elevated in cancer cells (Singh et al., 2022; Kim et al., 2019). PLK4 overexpression promotes the promiscuous assembly of multiple, nascent centrioles on the walls of mother centrioles (Fig. 1 A; [Peel et al., 2007; Bettencourt-Dias et al., 2005; Habedanck et al., 2005]). To determine whether a transcriptional response is associated with PLK4-induced centriole overduplication, we arrested RPE-1 cells in S phase and overexpressed PLK4 using an RPE-1-Tet-PLK4 Cetn2-GFP p53 WT cell line (Hatch et al., 2010). RNA sequencing was performed on samples isolated 16 h after PLK4 overexpression. Surprisingly, only three transcripts were elevated by >1.5-fold: *PLK4*, *UNK*, and *GALNT16*. The *UNK* mRNA transcript was elevated similarly to overexpressed *PLK4* (Fig. 1 B). The increase in *UNK* mRNA and its encoded protein in the PLK4-overexpressed cells was confirmed by single molecule, inexpensive FISH (smiFISH), western blot, and immunofluorescence (Fig. S1, A and B; and Data S1). In addition to the 103-kDa full length protein, a 55-kDa band recognized by the UNK antibody increased in intensity in PLK4-overexpressing cells and was decreased by UNK siRNA. This size does not match the 103 kDa of full-length UNK, nor known UNK isoforms, and is suggestive of a posttranslational modification or cleavage of UNK that is unique to PLK4-overexpressing cells (Fig. S1 B). Doxycycline-treated RPE-1 cells without PLK4 overexpression did not increase UNK protein (Fig. S1 B). We hypothesize that UNK upregulation upon PLK4 overexpression may occur through two models: increased transcription of the *UNK* gene or stabilization of *UNK* mRNA. PLK4 itself is not known to interact with nucleic acids, and the mechanism of increased *UNK* mRNA is unknown and requires further study. In summary, *UNK* transcript levels increase in response to PLK4 overexpression.

To determine if UNK protein functions at centrosomes, we visualized its subcellular localization. UNK largely localized to the cytoplasm (Murn et al., 2015; Murn et al., 2016), with a subpopulation localizing to the centrosome-proximal region (Fig. 1 C). Co-localization with centrin-labeled centrioles indicated that UNK resides near the distal ends of procentrioles, hereafter centrosome localization (Fig. 1 C and Fig. S1 C). mCherry-tagged UNK exhibited similar centrosome localization (Fig. S1 D). To quantify the localization of UNK, radial fluorescence intensity analysis, hereafter radial analysis, was performed for UNK in an 8-µm radius around the centrosome. The centroid of the centrosome was defined by the single brightest centrin centriole marker. Both cytoplasmic and centrosome levels of UNK increased upon PLK4 overexpression (Fig. 1 C and Fig. S1 C). The relative increase in UNK levels was greatest >6 µm from the centrosome. To quantify the change in UNK distribution upon PLK4 overexpression, UNK fluorescence after PLK4 overexpression was normalized as a ratio to UNK fluorescence at

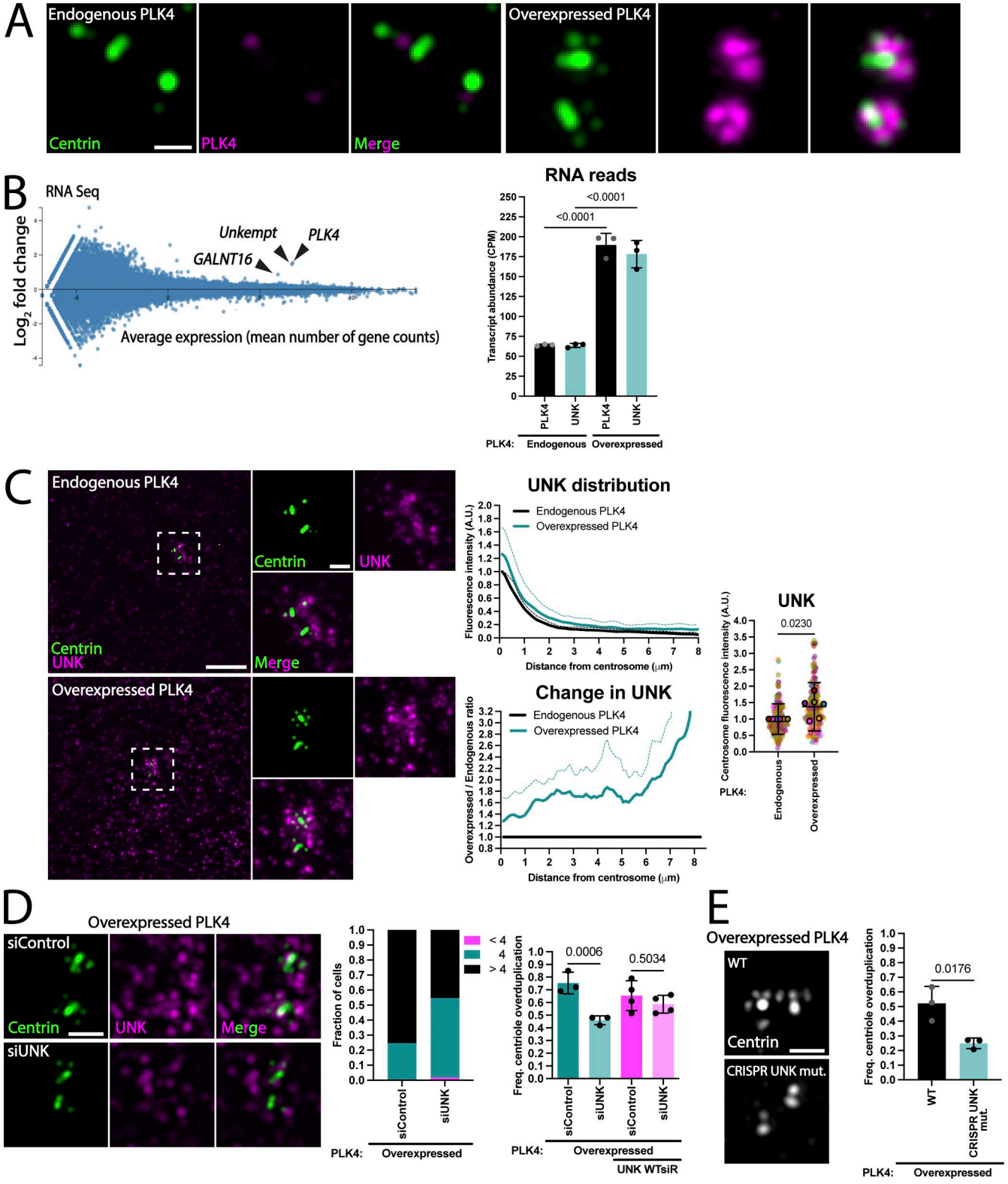

Figure 1. **The UNK RBP facilitates PLK4-induced centriole overduplication. (A)** PLK4 overexpression promotes centriole overduplication. Structured illumination microscopy (SIM) images of RPE-1-Tet-PLK4 Cetn2-GFP p53 WT cells with endogenous and overexpressed PLK4. PLK4, magenta, and centrioles (centrin), green. Scale bar, 0.5 µm. **(B)** *UNK* is elevated upon PLK4 overexpression. Left panel: $\log_2$ fold change versus mean expression intensity plot of mRNA levels based on RNA sequencing of RPE-1-Tet-PLK4 Cetn2-GFP p53 WT cells with overexpressed PLK4 16 h after overexpression in S phase. PLK4 and UNK transcripts are elevated by 1.5- and 1.4-fold, respectively. Right panel: Counts per million (CPM) of RNA reads of *PLK4* and *UNK* mRNAs in RPE-1-Tet-PLK4 Cetn2-GFP p53 WT cells with endogenous and overexpressed PLK4 in S phase. Graph values are expressed as the means of three biological replicates and SD. P values were determined using one-way ANOVA with Šídák post hoc test. **(C)** UNK protein is elevated at the centrosomal region upon PLK4 overexpression

in S phase. Left panels: SIM images of endogenous UNK in RPE-1-Tet-PLK4 Cetn2-GFP p53 WT cells with endogenous and overexpressed PLK4. UNK, magenta, and centrioles (centrin), green. Scale bar, 5 µm. Insets scale bar, 1 µm. Middle panels: 8-µm radial fluorescence intensity and corresponding ratio quantification of UNK using centrin as the centrosome centroid. Right panel: Centrosomal UNK mean normalized fluorescence intensity based on binned central 2 µm. Graph values are expressed as the means of six biological replicates of 25–30 cells per replicate and SD. P value was determined using an unpaired two-tailed *t* test. **(D)** UNK is required for PLK4-induced centriole overduplication. Left panels: SIM images of RPE-1-Tet-PLK4 Cetn2-GFP p53 WT cells showing centrioles in UNK-depleted cells with endogenous or overexpressed PLK4. UNK, magenta, and centrioles (centrin), green. Scale bar, 0.5 µm. Middle panel: Number of cells with greater than, equal to, and less than four centrioles (centrin; centriole overduplication). Graph values are expressed as the means of three and four biological replicates of 100 cells per replicate and SD. P values were determined using one-way ANOVA with the Šídák post hoc test. Right panel: Number of cells with greater than, equal to, and less than four centrioles (centrin; centriole overduplication). Graph values are expressed as the means of three and four biological replicates of 100 cells per replicate and SD. P values were determined using one-way ANOVA with the Šídák post hoc test. **(E)** CRISPR *UNK* mut. reduces centriole overduplication. Left panels: SIM images of RPE-1-Tet-PLK4 p53 KO UNK WT and *UNK* mut. showing centrioles with overexpressed PLK4 in S phase. Centrioles (not equally scaled) (centrin), grayscale. Scale bar, 1 µm. Right panels: Frequency of RPE-1-Tet-PLK4 p53 KO *UNK* WT and CRISPR *UNK* mut. cells with centriole overduplication in S phase. Graph values are expressed as the means of three biological replicates of 50–75 cells per replicate and SD. P values were determined using an unpaired two-tailed *t* test.

endogenous PLK4 levels (ratio analysis). UNK increased at the centrosomal area and in the cytoplasm. The centrosomal population of UNK, as defined as the radial 2 µm around the centrosome, increased by ∼40% upon PLK4 overexpression, following the dynamic centrosomal localization patterns of other centriolar satellites (Fig. 1 C; [Aydin et al., 2020]). Thus, UNK's centrosomal localization near centrioles increases upon PLK4-induced centriole overduplication.

To determine whether UNK is required for PLK4-induced centriole overduplication, S phase–arrested cells were depleted of UNK using siRNAs. UNK depletion reduced the frequency of cells with PLK4-induced centriole overduplication from 75% (siControl) to 45% (siUNK) (Fig. 1 D). UNK depletion using a second siRNA showed similar results (Fig. S1 E). Centriole overduplication was rescued by an siRNA-resistant (siR) mCherry-UNK in UNK siRNA-treated cells, suggesting that UNK is required for PLK4-induced centriole overduplication (Fig. 1 D). UNK siRNA depletion was more efficient in PLK4-overexpressed cells than endogenous PLK4 cells (45% depletion compared with 24% depletion). To test whether the residual UNK was sufficient to promote canonical centriole duplication, an UNK mutant *TP53* KO RPE-1 cell line was created by targeting the *UNK* gene using CRISPR/Cas9 (CRISPR *UNK* mut.; Fig. S1 F). Sequencing confirmed disruption of the *UNK* gene with indels that result in premature STOP codons in both alleles. Loss of UNK full-length protein was observed by western blot analysis (Fig. S1 F). UNK immunofluorescence staining in the CRISPR *UNK* mut. cells was strongly reduced. Signal observed was deemed nonspecific, as UNK protein was not detected in the western blot. Consistent with the siUNK, the CRISPR *UNK* mut. disrupted PLK4-induced centriole overduplication but not canonical centriole duplication (Fig. 1 E and Fig. S1 F). In summary, UNK facilitates PLK4-induced centriole overduplication but is dispensable for canonical centriole duplication.

UNK promotes the localization of centriole assembly factors

To elucidate how UNK facilitates PLK4-induced centriole overduplication, we asked whether UNK regulates the localization of centriole assembly proteins, including PLK4, that are required for centriole assembly (Coelho et al., 2015). S phase–arrested cells were depleted of UNK followed by PLK4 overexpression (Fig. 2 A). PLK4 protein at centrosomes was reduced by ∼35% in UNK knockdown (Fig. 2 B). Similarly, PLK4 protein was variably reduced by 28% in the CRISPR *UNK* mut. cells following PLK4 overexpression (Fig. S1 F). However, the total cellular levels of PLK4 were unchanged in UNK knockdown cells (Fig. S2 A and Data S2). This suggests that UNK facilitates centriole overduplication by promoting PLK4 localization to centrosomes.

To determine how UNK promotes PLK4 centrosome localization, we asked whether UNK modulates centriole proteins that recruit and anchor PLK4 to centrosomes. CEP63–CEP152, CEP192–CEP152 complexes, all recruit PLK4 (Brown et al., 2013; Sonnen et al., 2013). The mean centrosome fluorescence intensity of CEP63, CEP192, and CEP152 were all decreased upon knockdown of UNK (40%, 40%, and 20%, respectively; Fig. 2 B). We suggest this is the result of decreased recruitment of these proteins before centriole amplification; however, it is possible that the increase in WT cells is because of procentriole assembly. Surprisingly, a significant decrease in STIL was not observed in siUNK (Fig. 2 B) or CRISPR *UNK* mut. cells (Fig. S1 F). In summary, we propose that UNK promotes localization of early centriole assembly proteins required for PLK4 localization.

Centrin-positive puncta distributed throughout the cytoplasm were observed in UNK knockdown cells, regardless of PLK4 status (Fig. 2 C). These puncta were negative for other centriole (PLK4, CEP192, CEP152, or STIL) and centrosome (pericentrin or CDK5RAP2) proteins and did not nucleate MTs (Fig. S2 B), indicating they are not centrioles. The centrin puncta were, however, positive for centriolar satellite proteins (PCM1 and CEP131) (Fig. S2 C). This suggests that the centrin-positive puncta are a subset of the centriolar satellites dispersed from centrosomes.

UNK is a centriolar satellite protein and promotes the localization of PCM1 and CEP131

Centriolar satellites are non-membranous granules surrounding centrosomes that bind and transport proteins along MTs for centrosome assembly (Staples et al., 2012; Kodani et al., 2015; Kim et al., 2019) and ciliogenesis (Hall et al., 2013, 2023; Jewett et al., 2023; Stemm-Wolf et al., 2021). UNK was found in proximity labeling experiments using multiple centriolar satellite proteins as baits (Gupta et al., 2015). We confirmed that UNK is a centriolar satellite protein by colocalization with the centriolar satellite marker, CEP131 (Fig. 3 A). UNK colocalizes with a subset of CEP131-positive cytoplasmic and procentriole adjacent puncta.

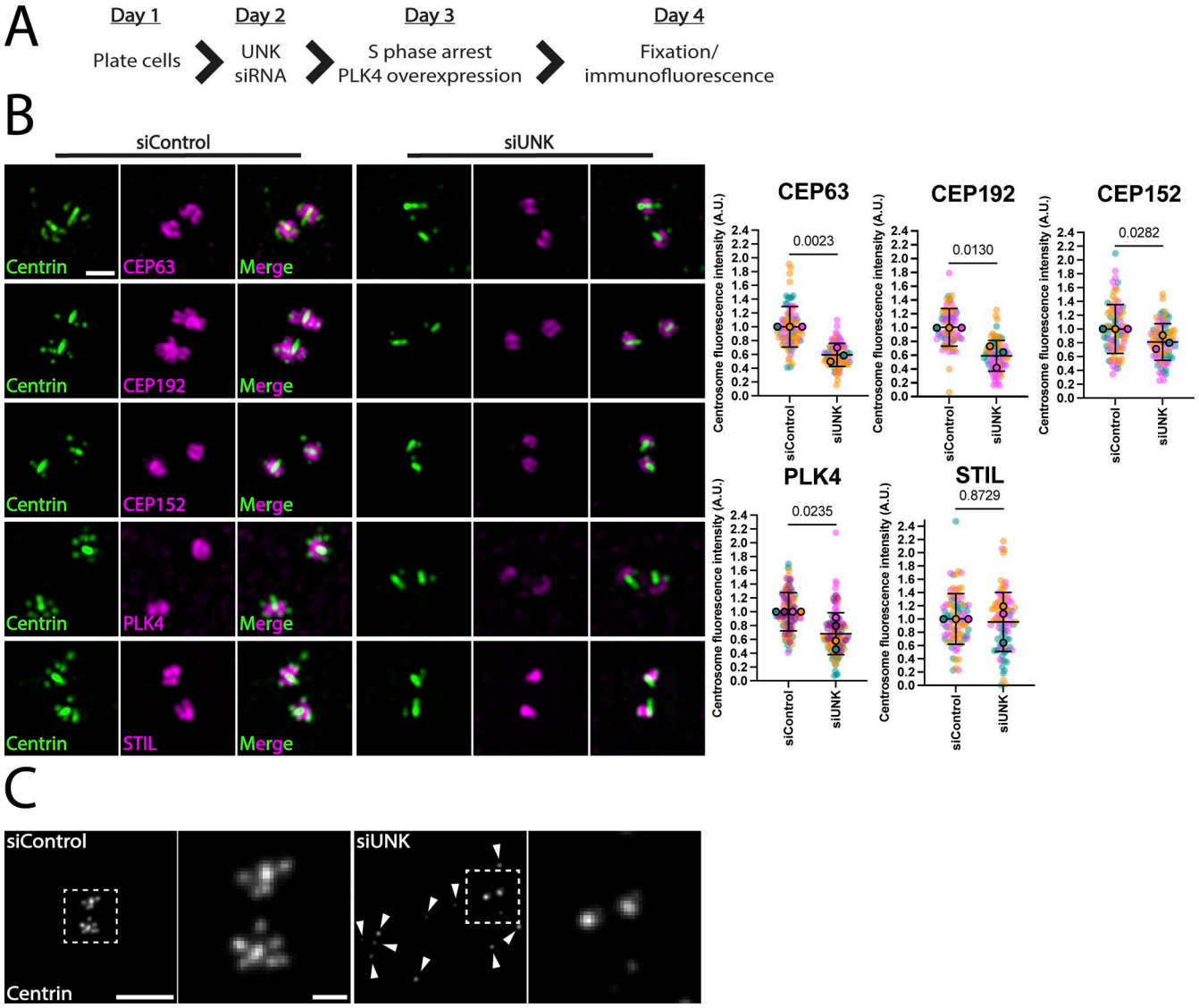

Figure 2. **UNK promotes the localization of centriole assembly protein factors. (A)** Schematic showing experimental timeline for UNK depletion, S phase arrest, PLK4 overexpression, and fixation for immunofluorescence. **(B)** Centriole assembly protein localization is reduced in siUNK cells. Left panels: SIM images of RPE-1-Tet-PLK4 Cetn2-GFP p53 WT cells showing fluorescence at centrosomes in UNK-depleted cells with overexpressed PLK4 in S phase. CEP63, CEP192, CEP152, PLK4, and STIL are magenta, and centrioles (centrin) are green. Scale bar, 1.0 µm. Right panels: Mean normalized centrosome fluorescence intensities of centriolar proteins. Graph values are expressed as the means of three and four biological replicates of 25–30 cells per replicate and SD. P values were determined using an unpaired two-tailed *t* test. **(C)** UNK depletion promotes ectopic centrin-positive foci. Confocal images of RPE-1-Tet-PLK4 Cetn2-GFP p53 WT cells showing centrin-positive foci in UNK-depleted cells with overexpressed PLK4 in S phase. Centrioles (centrin), grayscale. Arrows indicate sites of ectopic centrin foci. Scale bar, 5 µm. Insets scale bar, 1 µm.

We next asked how CEP131 and UNK localization changes during PLK4-induced procentriole assembly. Centriole overduplication and PLK4 protein were observed after PLK4 overexpression and reached a maximum by 12 h (Fig. S2 D). To capture the dynamics of UNK and CEP131 protein localization and levels, cells were analyzed at 6 and 12 h after PLK4 overexpression. UNK levels increased at the centrosome region 6 and 12 h (45%) after PLK4 overexpression (Fig. 3 B). CEP131 exhibited a modest increase at centrosomes (20% and 25%) at 6 and 12 h after PLK4 overexpression, respectively (Fig. 3 B). Thus, UNK and CEP131 increase at the centrosomal region at early stages of PLK4-induced centriole overduplication.

We next asked if UNK regulates centriolar satellites. UNK knockdown decreased centrosomal localization of PCM1 and CEP131 centriolar satellite proteins causing dispersal throughout the cytoplasm (Fig. 3 C, Fig. S1 F, and Fig. S2 C). This redistribution of PCM1 and CEP131 upon UNK knockdown was independent of PLK4 overexpression (Fig. S2 C). The total cellular levels of PCM1 and CEP131 did not change upon UNK depletion (Fig. S2 E). Thus, UNK promotes the localization of PCM1- and

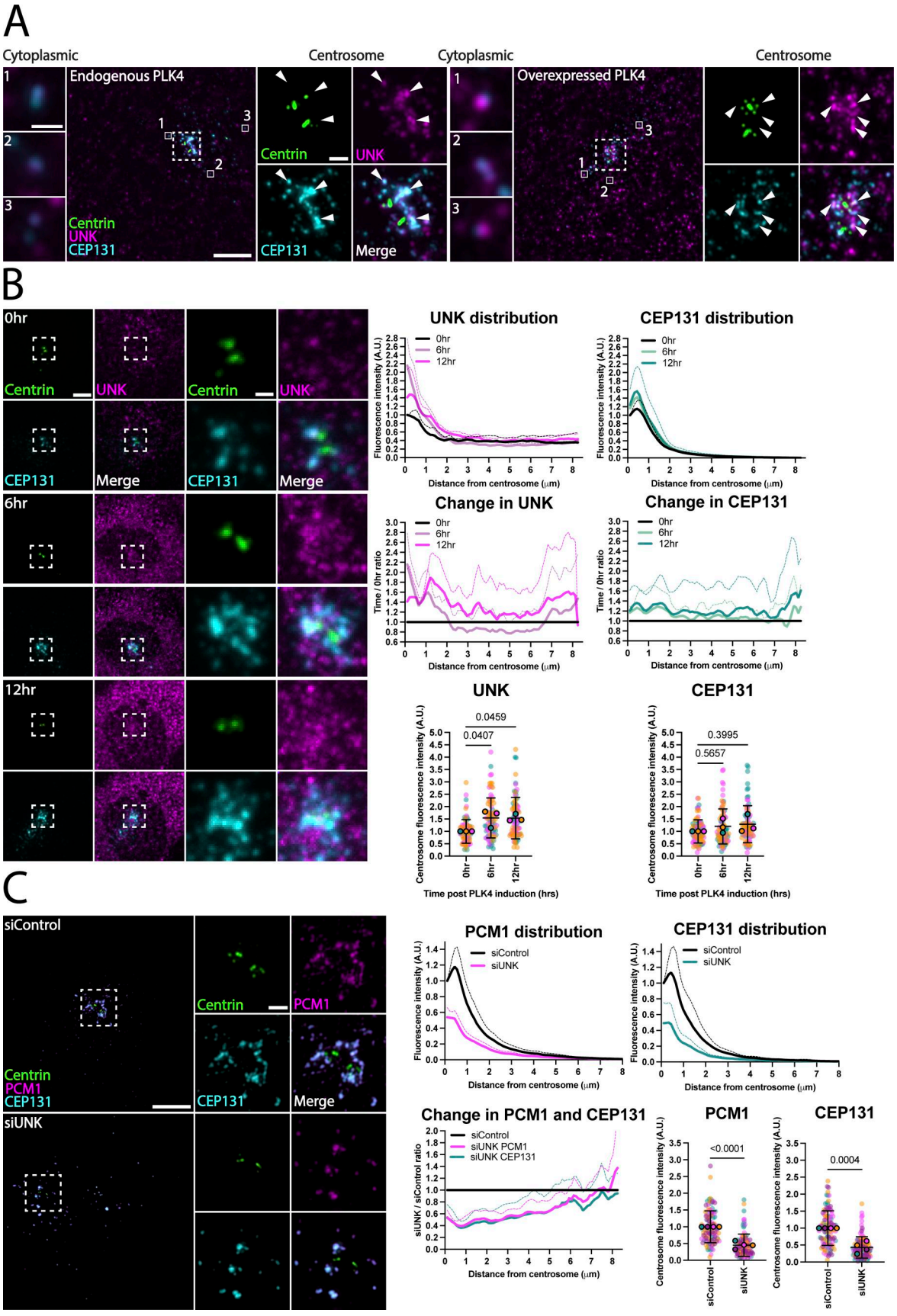

Figure 3. **UNK is a centriolar satellite protein and promotes PCM1 and CEP131 localization. (A)** UNK localizes to CEP131-positive centriolar satellites. SIM images of RPE-1-Tet-PLK4 Cetn2-GFP p53 WT cells showing UNK protein localization with endogenous and overexpressed PLK4 in S phase. UNK, magenta;

CEP131, cyan; centrioles (centrin), green. Arrows indicate sites of UNK and CEP131 colocalization. Scale bar, 5 µm. Left insets scale bar, 0.5 µm. Right insets scale bar, 1 µm. **(B)** PLK4 overexpression promotes UNK localization to centrosomes in a time-dependent manner. Left panels: Confocal images of RPE-1-Tet-PLK4 Cetn2-GFP p53 WT cells showing UNK and CEP131 localization 6 and 12 h after PLK4 overexpression in S phase. UNK, magenta; CEP131, cyan; centrioles (centrin), green. Scale bar, 5 µm. Insets scale bar, 1 µm. Right top and middle panels: 8-µm radial fluorescence intensity and corresponding ratio quantification of UNK and CEP131 using centrin as the centrosome centroid. Right bottom—mean normalized centrosomal UNK and CEP131 fluorescence intensity based on binned central 2 µm. Graph values are expressed as the mean of three biological replicates of 25–30 cells per replicate and SD. P values were determined using one-way ANOVA with the Dunnett post hoc test. **(C)** Centriolar satellites are dispersed from centrosomes in siUNK cells with overexpressed PLK4. Left panels: SIM images of RPE-1-Tet-PLK4 Cetn2-GFP p53 WT cells showing centriolar satellites and their localization to the centrosomes in UNK-depleted cells with overexpressed PLK4 in S phase. PCM1, magenta; CEP131, cyan; centrioles (centrin), green. Scale bar, 5 µm. Insets scale bar, 1 µm. Right top panels: 8-µm radial fluorescence intensity of PCM1 and CEP131 using centrin as the centrosome centroid. Right, bottom left panels: 8 µm ratio quantification of PCM1 and CEP131 using centrin as the centroid. Right, bottom right panels: Centrosome PCM1 and CEP131 mean normalized fluorescence intensity based on binned central 2 µm. Graph values are expressed as the means of four biological replicates of 25–30 cells per replicate and SD. P values were determined using an unpaired two-tailed *t* test.

CEP131-positive centriolar satellites to centrosomes but does not affect their cellular levels (Fig. 3 C and Fig. S2 E).

CEP131, but not PCM1, promotes PLK4-induced centriole overduplication

Because UNK promotes centrosome localization of both PCM1- and CEP131-positive centriolar satellites (Fig. 3 C) and facilitates PLK4-induced centriole overduplication (Fig. 1 D), we asked if these proteins regulate PLK4-induced centriole overduplication. PCM1, CEP131, or both were knocked down in PLK4 overexpressing, S phase–arrested cells and knockdown efficiency at the centrosome was assessed for both proteins (Fig. S3 B). PCM1 knockdown did not affect the frequency of cells with overduplicated centrioles. In contrast, CEP131 knockdown and the double knockdown attenuated centriole overduplication to ∼45% and 32%, respectively (Fig. 4 A). This is consistent with prior reports showing that loss of PCM1 does not affect centriole amplification in multiciliated cells (Hall et al., 2023), while CEP131 knockdown does suppress PLK4-induced centriole overduplication (Hall et al., 2023; Kim et al., 2019; Staples et al., 2012). This suggests different roles for PCM1 and CEP131 in centriole assembly. Moreover, knockdown of PCM1 modestly increased the centrosomal localization of CEP131 and UNK, whereas knockdown of CEP131 decreased the localization of PCM1 (Staples et al., 2012; Hall et al., 2023) and UNK (Fig. 4, A and C). Furthermore, knockdown of CEP131 and double knockdown modestly affected canonical centriole duplication (Fig. S3 B). In summary, knockdown of CEP131, but not PCM1, decreases centriole duplication. This suggests that UNK's role in PLK4-induced centriole overduplication occurs in coordination with CEP131, but not PCM1.

To elucidate how PCM1 and CEP131 differentially regulate PLK4-induced centriole overduplication, we quantified centrosome localization of the centriole assembly proteins CEP192, CEP152, PLK4, and STIL in PCM1, CEP131, or double knockdown (Fig. 4 B). PCM1 knockdown only reduced PLK4 at centrosomes but did not affect centriole overduplication, suggesting that the partial loss of PLK4 may not negatively affect centriole assembly or that other mechanisms compensate for this decrease in PLK4. Conversely, CEP131 knockdown reduced CEP192, CEP152, and PLK4 at centrosomes.

CEP131 knockdown decreased STIL at centrosomes by 40%, whereas PCM1 knockdown modestly increased centrosome localized STIL (Fig. 4 B). This suggests that both centriolar satellite proteins uniquely promote the localization of procentriole assembly proteins to the centrosome, but only CEP131 robustly promotes the localization of STIL. PLK4 phosphorylates STIL to recruit proteins necessary for centriole assembly (Moyer and Holland, 2019; Dzhindzhev et al., 2017; Ohta et al., 2014). The loss of STIL upon CEP131 depletion suggests this may attenuate centriole overduplication when CEP131 is lost. Because UNK knockdown reduces centrosomal CEP131 levels (Fig. 3 C), it would be expected that it also decreases STIL. We did not observe a significant change to STIL levels in UNK knockdown or CRISPR *UNK* mut. cells (Fig. 2 B and Fig. S1 F). We suggest this is because UNK loss does not completely disrupt CEP131 localization and function. Alternatively, this may identify unique roles for UNK and CEP131 in centriole assembly and stability. Understanding the unique and overlapping functions of UNK and CEP131 will require future study.

Because CEP131 and UNK knockdown both attenuate centriole overduplication, we asked if CEP131 or PCM1 regulate UNK localization. CEP131 knockdown reduced UNK levels at centrosomes (Fig. 4 C), suggesting that UNK and CEP131 are codependent for their localization to centrosomes. Conversely, PCM1 knockdown increased UNK proximity to centrioles, even though the overall centrosomal levels of UNK were not affected (Fig. 4 C). Thus, UNK and CEP131 localization are interdependent and suggests their localization near assembling centrioles promotes centriole overduplication.

UNK's RNA-binding domain is required for PLK4-induced centriole overduplication

UNK's RNA-binding domain, composed of six zinc fingers in the N terminus, is required for RNA binding and UNK's control of cell morphology (Murn et al., 2015; Murn et al., 2016). We asked if UNK RNA-binding is required for PLK4-induced centriole overduplication. Cells were depleted of endogenous UNK, and an siR, N-terminal mCherry tag, WT (WTsiR), or RNA-binding mutant (Mut.siR) were expressed in S phase–arrested cells, concurrent with PLK4 overexpression (Fig. 5 A). The Mut.siR was generated by mutating R119, Y120, N143, F149, Q288, F289, R310, and F316 residues to alanine, as previously shown to abrogate trinucleotide RNA binding (Murn et al., 2016). Both WTsiR and Mut.siR proteins localize to centrosomes (Fig. S3 A). Depletion of endogenous UNK and expression of WTsiR, but not Mut.siR, with 0.4 µg/ml doxycycline rescued centriole overduplication (Fig. 5 A). Surprisingly, expression of WTsiR with

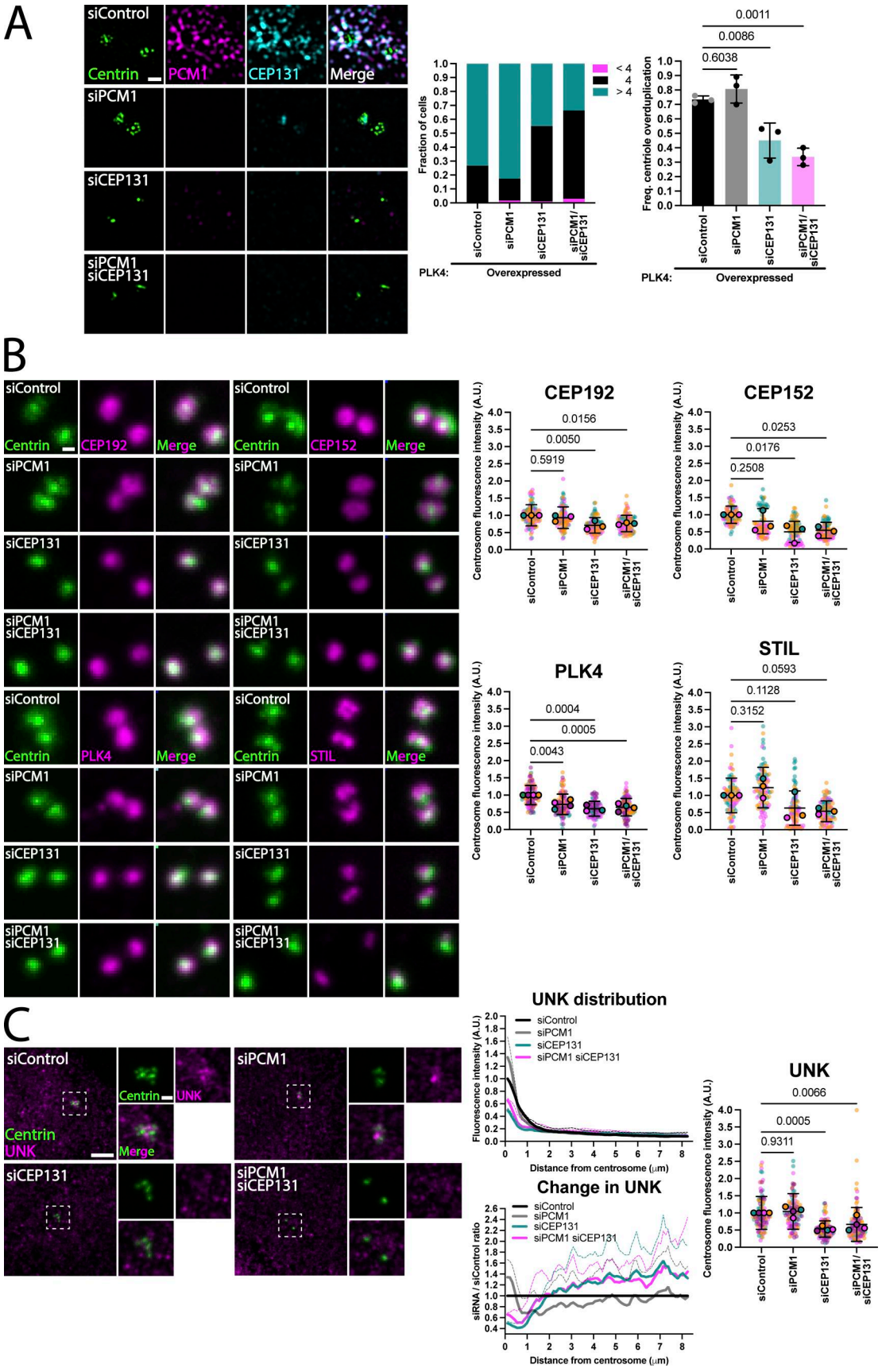

Figure 4. **CEP131, but not PCM1, promotes PLK4-induced centriole overduplication. (A)** CEP131 promotes PLK4-induced centriole overduplication. Left panels: SIM images of RPE-1-Tet-PLK4 Cetn2-GFP p53 WT cells showing centrioles in PCM1, CEP131, or double-depleted cells with overexpressed PLK4 in S

phase. PCM1, magenta; CEP131, cyan; centrioles (centrin), green. Scale bar, 1.0 µm. Middle panel: Number of cells with greater than, equal to, and less than four centrioles (centrin; centriole overduplication). Right panel: Frequency of cells with centriole overduplication. Graph values are expressed as the means of three biological replicates of 100 cells per replicate and SD. P values were determined using one-way ANOVA with the Dunnett post hoc test. **(B)** CEP131 and PCM1 depletion disrupts centriolar protein localization to the centrosome. Left panels: Confocal images of RPE-1-Tet-PLK4 Cetn2-GFP p53 WT cells showing centriolar protein localization in PCM1, CEP131, or double-depleted cells with overexpressed PLK4 in S phase. CEP192, CEP152, PLK4, and STIL are magenta, and centrioles (centrin) are green. Scale bar, 0.5 µm. Right panels: Mean normalized centrosome fluorescence intensities of centriolar proteins. Graph values are expressed as means of three and four biological replicates of 25–30 cells per replicate and SD. P value was determined using one-way ANOVA with the Dunnett post hoc test. **(C)** CEP131-positive centriolar satellites are required for UNK localization to centrosomes. Left panels: Confocal images of RPE-1-Tet-PLK4 Cetn2-GFP p53 WT cells showing UNK localization in PCM1, CEP131, or double-depleted cells with overexpressed PLK4 in S phase. UNK, magenta, and centrioles (centrin), green. Scale bar, 5 µm. Insets scale bar, 1 µm. Middle panels: 8-µm radial fluorescence intensity and corresponding ratio quantification of UNK using centrin as the centrosome centroid. Right panels: Mean normalized centrosomal UNK fluorescence intensity based on binned central 2 µm. Graph values are expressed as the means of four biological replicates of 25–30 cells per replicate and SD. P values were determined using one-way ANOVA with the Dunnett post hoc test.

1.0 µg/ml doxycycline, but not Mut.siR (without siUNK treatment), blocked centriole overduplication (Fig. S3 C). This suggests that centriole overduplication requires UNK RNA binding and demonstrates that too much UNK RNA binding hinders centriole overduplication. Neither expression of WTsiR nor Mut.siR rescued CEP131-positive centriolar satellite localization to the centrosome (Fig. 5 B and Fig. S3 D). These results suggest (1) low levels of WT UNK expression are sufficient to partially rescue PLK4-induced centriole overduplication in siUNK, whereas high levels of WT UNK suppress centriole assembly; (2) UNK's RNA-binding domain is required for PLK4-induced centriole overduplication; and (3) expression of WT UNK in UNK-depleted cells does not rescue centriolar satellite localization to the centrosome. This latter result requires future studies to uncover the relative contributions of UNK and CEP131 in centriole assembly. In summary, UNK RNA binding is important for PLK4-induced centriole overduplication.

UNK and centriolar satellites promote local translation at and around centrosomes

Because UNK regulates mRNA translation (Murn et al., 2015; Murn et al., 2016; Shah et al., 2024) and localizes to centrosomes and centriolar satellites, we investigated local translation at these structures. Cells were labeled with O-propargyl-puromycin (OPP), a puromycin analog that enters the ribosome acceptor site and is incorporated into nascent polypeptides. This modification can be fluorescently labeled to mark sites of translation (Staudacher et al., 2021). RPE-1 cells were S phase arrested, induced for PLK4 overexpression for 16 h, labeled with OPP, and co-stained with CEP131. OPP signal was observed throughout the cytoplasm and at and around centrosomes (Fig. 5 C and Fig. S3 E), partially colocalizing with centrin-positive centrioles and CEP131-positive centriolar satellites (Fig. 5 C). The OPP signal at centrosomes decreased at early 6 and 12 h time points and then increased 16 h after PLK4 overexpression (Fig. S3 F and Fig. 5 D). Overexpression of GFP alone did not change centrosome OPP levels, indicating the change in OPP signal is not due to doxycycline induction of expression (Fig. S3 G). Furthermore, inhibiting translation with cycloheximide disrupted OPP labeling (Fig. S3 E). To assess whether translation suppression affects centriole overduplication, RPE-1 cells were S phase arrested, induced for PLK4 overexpression, and subsequently treated with cycloheximide. Treatment with cycloheximide suppressed centriole overduplication (Fig. S3 H), suggesting that centriole overduplication requires translation. In summary, centrosomes and CEP131-positive centriolar satellites surrounding centrosomes are sites of active translation during S phase. OPP labels truncated nascent polypeptides that are released from the ribosome, and the possibility of diffusion or trafficking of these labeled polypeptides to the centrosome cannot be eliminated (Enam et al., 2020). Regardless, these results show that newly synthesized proteins localize to centrosomes and centriolar satellites in response to PLK4 overexpression, and translation is required for centriole overduplication. This is consistent with the mRNAs, RBPs, and translation machinery detected around centrosomes (Filippova et al., 2012; Pascual et al., 2021; Ishigaki et al., 2014).

UNK was previously shown to suppress translation (Murn et al., 2015; Murn et al., 2016; Shah et al., 2024). Moreover, UNK localizes to the centrosome during early centriole assembly and remains enriched at the centrosomes 6, 12, and 16 h after PLK4 overexpression (Fig. 3 B and Fig. 1 C). To determine whether UNK regulates translation at and around centrosomes, we depleted UNK and quantified OPP signal at centrosomes after PLK4 overexpression. UNK depletion decreased centrosome translation by 35% without altering the levels of global translation at 16 h (Fig. 5 E and Fig. S3 J), but did not affect centrosomal OPP at 6 h (Fig. S3 K). Because UNK promotes the localization of centriolar satellites (Fig. 3 C) and centriolar satellites are sites of translation (Fig. 5 C), we asked whether centriolar satellites regulate local translation at centrosomes. To test this, PCM1, CEP131, or both were depleted, and the OPP signal at centrosomes was quantified. Consistent with UNK depletion, CEP131, but not PCM1, depletion decreased centrosome translation by 55% at 16 h, but not at early time points (Fig. 5 F and Fig. S3 L). This is consistent with the second most abundant Gene Ontology category for protein regulatory functions interacting with PCM1 and CEP131 being RNA regulatory processes (Fig. S3 I; [Gheiratmand et al., 2019]). UNK and CEP131 centriolar satellite proteins interact with translation machinery, including initiation and elongation factors, ribosomal proteins, and poly A–binding proteins (Gheiratmand et al., 2019). The variability of OPP at 6 and 12 h in UNK- and CEP131-depleted cells may be due to incomplete knockdown of either protein, which was not assessed. These data suggest that UNK and centriolar satellites cooperate to promote local translation at centrosomes. The observed effect of UNK on promoting localized translation at the centrosome is distinct from its canonical translation suppression role but may

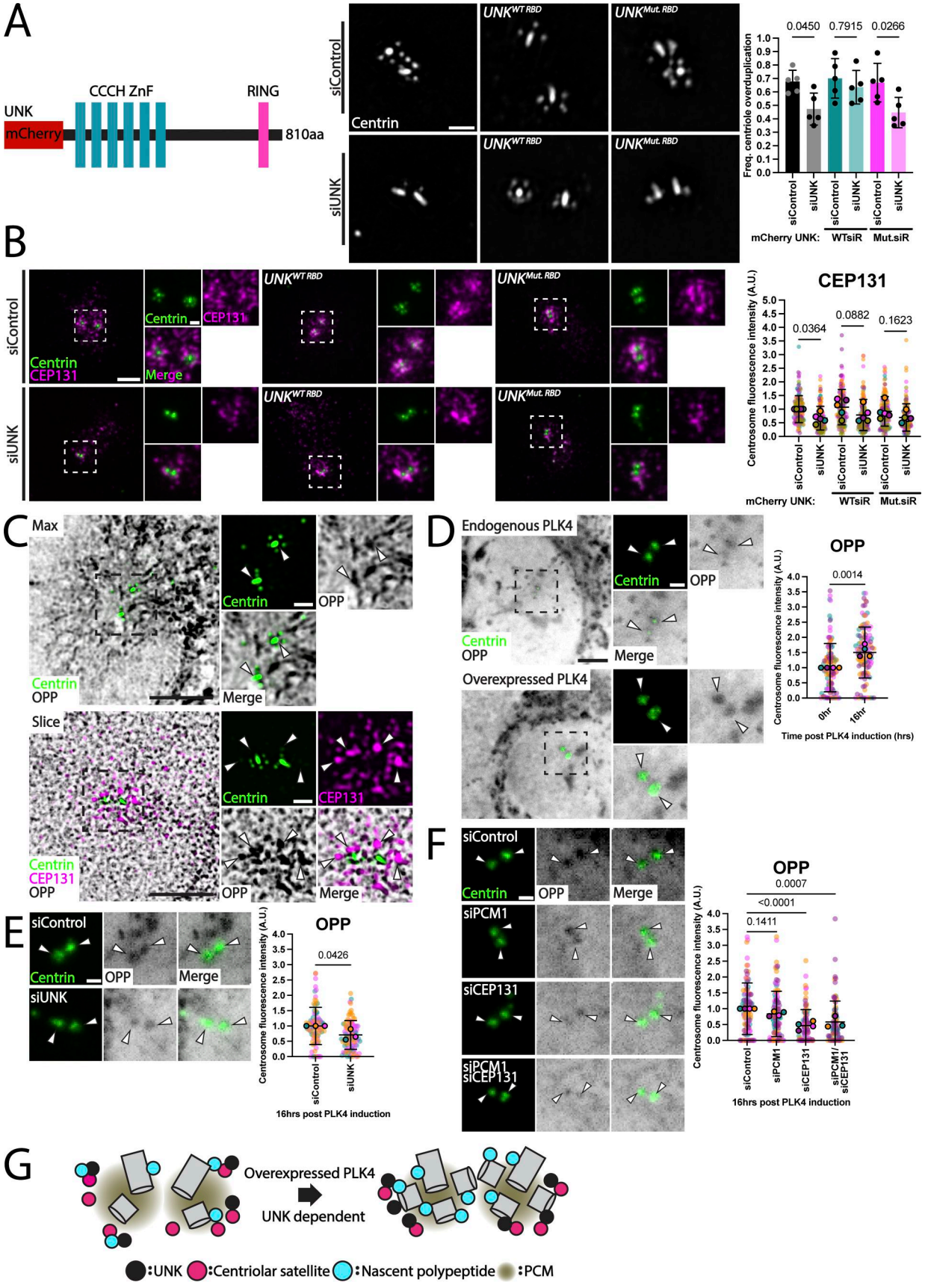

Figure 5. **UNK's RNA-binding domain is required for PLK4-induced centriole overduplication. (A)** UNK RNA binding is required for centriole overduplication. Left panels: Schematic of mCherry-UNK protein. Middle panels: SIM images of RPE-1-Tet-PLK4 Cetn2-GFP p53 WT cells showing centrioles in UNK-

depleted cells with overexpressed PLK4 and expression of either siR UNK (WTsiR or Mut.siR) in S phase. Centrioles (centrin), grayscale. Scale bar, 1 µm. Right panel: Frequency of cells with centriole overduplication (centrin; centriole overduplication). Graph values are expressed as the means of five biological replicates of 100 cells per replicate and SD. P values were determined using one-way ANOVA with the Šídák post hoc test. **(B)** UNK RNA binding is dispensable for CEP131-positive centriolar satellite localization. Left panels: Confocal images of RPE-1-Tet-PLK4 Cetn2-GFP p53 WT cells showing CEP131 localization in UNK-depleted cells with overexpressed PLK4 and expression of either WTsiR or Mut.siR UNK in S phase. CEP131, magenta, and centrioles (centrin), green. Scale bar, 5 µm. Insets scale bar, 1 µm. Right panel: Centrosomal CEP131 mean normalized fluorescence intensity based on binned central 2 µm. Graph values are expressed as the means of five biological replicates of 25–30 cells per replicate and SD. P values were determined using one-way ANOVA with the Fisher's least significant difference (LSD) post hoc test. **(C)** Nascent protein synthesis is enriched at centrosomes and centriolar satellites. Top panel: SIM images showing centrosome localization of OPP in RPE-1-Tet-PLK4 Cetn2-GFP p53 WT cells with overexpressed PLK4 in S phase. OPP, grayscale, and centrioles (centrin), green. Arrows indicate sites of OPP signal. Scale bar, 5 µm. Insets scale bar, 1 µm. Bottom panel: SIM single slice image showing centriolar satellite localization of OPP in RPE-1-Tet-PLK4 Cetn2-GFP p53 WT cells with overexpressed PLK4 in S phase. CEP131, magenta; OPP, grayscale; centrioles (centrin), green. Arrows indicate sites of OPP signal. Scale bar, 5 µm. Insets scale bar, 1 µm. **(D)** PLK4 overexpression causes increased translation at centrosomes during late centriole assembly. Left panels: Confocal images of RPE-1-Tet-PLK4 Cetn2-GFP p53 WT cells showing centrosome staining of OPP 16 h after PLK4 overexpression in S phase. OPP, grayscale, and centrioles (centrin), green. Arrows indicate sites of OPP signal. Scale bar, 5 µm. Insets scale bar, 1 µm. Right panel: Mean normalized centrosome fluorescence intensities of OPP. Graph values are expressed as the means of four biological replicates of 25–30 cells per replicate and SD. P value was determined using an unpaired two-tailed *t* test. **(E)** UNK promotes translation at centrosomes during late centriole assembly. Left panels: Confocal images of RPE-1-Tet-PLK4 Cetn2-GFP p53 WT cells showing centrosome staining of OPP in UNK-depleted cells 16 h after PLK4 overexpression in S phase. OPP, grayscale, and centrioles (centrin), green. Arrows indicate sites of OPP signal. Scale bar, 1 µm. Right panel: Mean normalized centrosome fluorescence intensities of OPP. Graph values are expressed as the means of three biological replicates of 25–30 cells per replicate and SD. P value was determined using an unpaired two-tailed *t* test. **(F)** Centriolar satellites promote local translation at centrosomes during late centriole assembly. Left panels: Confocal images of RPE-1-Tet-PLK4 Cetn2-GFP p53 WT cells showing centrosome staining of OPP in cells with PCM1, CEP131, or double-depleted cells 16 h after PLK4 overexpression in S phase. OPP, grayscale, and centrioles (centrin), green. Arrows indicate sites of OPP signal. Scale bar, 1 µm. Right panel: Mean normalized centrosome fluorescence intensities of OPP. Graph values are expressed as the means of three and four biological replicates of 25–30 cells per replicate and SD. P values were determined using one-way ANOVA with the Dunnett post hoc test. **(G)** Model of UNK facilitating PLK4-induced centriole overduplication with centriolar satellites and localized translation at the centrosomes.

elucidate a specialized role of RBPs at subcellular compartments like the centrosome.

In summary, nascent protein synthesis decreases at and around centrosomes early (6–12 h) during PLK4-induced centriole duplication but then is elevated at late time points (16 h). This latter activation of centrosome translation is promoted, in part, by UNK and CEP131.

Discussion

PLK4 overexpression increases UNK, which acts as a PLK4 co-factor for centriole overduplication. The *UNK* transcript is one of the few changed by PLK4 overexpression, suggesting that centriole overduplication mostly utilizes posttranscriptional mechanisms. UNK is an RBP that, in coordination with CEP131-positive centriolar satellites, facilitates centriole overduplication and affects the regulation of local translation at centrosomes. While the detailed interplay between PLK4, UNK, CEP131, and centrosome translation requires further study, we reveal a novel role for the UNK RBP in promoting PLK4-induced centriole overduplication.

Centriolar satellites are reported to have both positive and negative effects on centriole duplication (Aydin et al., 2020; Stemm-Wolf et al., 2021). Here, the attenuation of PLK4-dependent centriole overduplication was observed upon UNK and CEP131, but not PCM1, knockdown, suggesting centriolar satellite constituents scaffolded or regulated by UNK and CEP131 contribute to centriole overduplication. UNK is dispensable for canonical centriole duplication but important for PLK4-induced centriole overduplication, while CEP131 mildly affects canonical centriole duplication and is important for PLK4-induced centriole overduplication (Fig. S1 F and Fig. S3 B; [Denu et al., 2019; Kim et al., 2019; Stemm-Wolf et al., 2021]). Consistent with our data, UNK is upregulated in cancers with PLK4 overexpression and centriole overduplication (DepMap; [Tsherniak et al., 2017]). Our finding that UNK promotes CEP131 accumulation at centrosomes during PLK4 induction suggests a 2-level positive feedback loop through which PLK4 overexpression acts. By increasing UNK, more CEP131 is recruited to centrosomes whose phosphorylation by PLK4 in turn stabilizes PLK4 at the centrioles (Denu et al., 2019; Staples et al., 2012). Because UNK recruits CEP131 to centrosomes, UNK may promote centriole duplication through CEP131-positive centriolar satellite localization. This is consistent with our observations that PLK4 levels decrease upon UNK and CEP131 knockdown.

Finding UNK at centriolar satellites around centrosomes, we examined whether its established function as a translational regulator was involved in centriole overduplication (Murn et al., 2015; Murn et al., 2016; Shah et al., 2024). We found local translation occurs at centriolar satellites using the global translational marker, OPP. In support of this finding, translation machinery also localizes around centrosomes (Kwon et al., 2021; Sepulveda et al., 2018), and proteomic studies identify translation machinery and other RBPs associated with centriolar satellites (Gupta et al., 2015; Gheiratmand et al., 2019; Arslanhan et al., 2020). In mouse tracheal multiciliated cells, newly synthesized peptides colocalize with PCM1-positive apical granules during centriole amplification (Liu et al., 2023). This supports the notion that centriolar satellites are sites of local translation.

To establish a role for UNK in centrosomal local translation, a baseline of the centrosomal translation profile during PLK4-induced centriole overduplication was established. This revealed a dynamic program of centrosome translation, which decreases early in centriole assembly (6 h post PLK4 induction) and then increases above its starting point (16 h post PLK4 induction). This leads us to speculate that translation of negative centriole assembly regulators is suppressed to support centriole assembly early in the assembly process. Neither UNK nor CEP131

appear to affect early translational suppression as detected by OPP, though they may be responsible for translational regulation of specific mRNAs beyond the resolution of this study (Gupta et al., 2015; Gheiratmand et al., 2019). In future studies, it will be interesting to examine the centrosomal translation program during canonical centriole biogenesis in live cells. Transient UNK and CEP131 knockdown negatively affect the increased translation that occurs late in centriole overduplication, though we do not detect changes to translation suppression that is observed during early centriole assembly. Interestingly, RBP-mediated translational suppression is required for mRNA trafficking in neurons (Das et al., 2021). If UNK is required for translation suppression at centriolar satellites to facilitate satellite trafficking, then disruption of UNK may affect centriolar satellite distribution, as is observed when UNK is depleted. Translation suppression during early centriole overduplication may be mediated by other components of the translational suppression machinery. In support of this idea, the translation suppressor complex CCR4–NOT (Kadyrova et al., 2007; Bhandari et al., 2014; Duchaine and Fabian, 2019; Leppek et al., 2013; Du et al., 2016) associates with centrioles and centriolar satellites (Youn et al., 2018; Gupta et al., 2015; Gheiratmand et al., 2019). UNK is reported to suppress translation of mRNAs through the CCR4–NOT complex, primarily through direct interaction with CNOT9 (Shah et al., 2024). In support of the centrosome-specific translation suppression model, knockdown of CNOT1 leads to translationally upregulated mRNAs that encode centrosome proteins (Gillen et al., 2021). Further, localized translation suppression may be required for macromolecular structure assembly and organization. Indeed, the CNOT1 ortholog in *Caenorhabditis elegans*, LET-711, localizes to centrosomes and regulates spindle positioning and MT length (DeBella et al., 2006). Future studies require the examination of CCR4–NOT localization and its effect on centriole duplication and centriolar satellite organization.

In summary, we demonstrate an increase in *UNK* mRNA and protein upon PLK4 overexpression that results in positive feedback between UNK and PLK4 protein localization to centrosomes. Translation is regulated at centrosomes during PLK4-induced centriole overduplication and is mediated, in part, by UNK and CEP131 that have roles in promoting centriole overduplication. Because UNK supports PLK4-induced centrosome overduplication but is dispensable for canonical centrosome duplication, it is a potential novel target for centrosome amplified cancer cells worthy of further study.

Materials and methods

Cell culture growth conditions and siRNA treatments

RPE-1-Tet-PLK4 Cetn2-GFP p53 WT (a kind gift from M.B. Tsou; Sloan Kettering Cancer Center, New York, NY, USA [Hatch et al., 2010]) was grown in DMEM/F12 with glutamine (Cytiva or Life Technologies) with 10% tetracycline-free FBS (Peak Serum) supplemented with penicillin and streptomycin (Life Technologies) at 37°C with 5% CO_2. A PCR test for mycoplasma contamination was performed every 6 mo. For PLK4 overexpression experiments, cells were plated onto 12-mm circular cover glass, no. 1.5 (Electron Microscopy Sciences), coated with collagen (C9791; Sigma-Aldrich) in 24-well plates at 12,500 cells and 7,000 cells for 48- and 72-h knockdown, respectively. The following day, cells were treated with siRNAs using the Lipofectamine RNAiMAX Transfection Reagent (Thermo Fisher Scientific) following the manufacturer's instructions. Transfection complexes were removed from cells 5–6 h after addition, and cells were provided fresh medium. 24 h prior to fixation, cells were arrested with 1.5 µg/ml aphidicolin (Cayman Chemical Company). PLK4 was induced with 1.0 µg/ml doxycycline (Sigma-Aldrich) 8 h after initiation of the aphidicolin arrest. siRNAs used were siControl: Mission siRNA Universal Negative Control #1 SIC001 (Sigma-Aldrich) 50 nM, CEP131: Stealth HSS146116, 5′-CAGAGUGCCAGGAAUGCGGCAGCCU-3′ 50 nM. For PCM1 knockdown, ON-TARGET siRNAs were used in combination J-005165-07: 5′-GCGCCUUACUCAUCUAAUA-3′ 25 nM and J-005165-09: 5′-AGAAUAAUGUUCAGAGGUU-3′; Dharmacon 25 nM.

Generation of UNK siR constructs

To generate WTsiR and Mut.siR UNK constructs, 1.8-kb gene blocks (Integrated DNA Technologies [IDT]) encompassing the N terminal region of UNK, six Zinc fingers, and siRNA target regions were synthesized. Zinc finger residues, previously shown to abrogate UNK RNA binding when mutated to alanine (Murn et al., 2016) (R119A, Y120A, N143A, F149A, Q288A, F289A, R310A, and F316A), were utilized for Mut.siR UNK. For generating siRNA resistance toward two different siRNAs, synonymous codon-optimized mutations were made to siRNA #1 (HSS150335; Thermo Fisher Scientific), 5′-GTGCCCTCCTCTGTAGAAACA GCAG-3′, and siRNA #2 (pool of 4 siRNAs) (M-022950-01-0010; Horizon Discovery siGENOME), 5′-CCTGAAAGAATTCCGCAC A-3′, 5′-AAGCACAAATACAGGTCGT-3′, 5′-CCACCAAGTGCA ACGACAT-3′, and 5′-GGAGAAGACTTTCGATAAC-3′ targets. To generate WTsiR and Mut.siR UNK, human UNK was first amplified from cDNA (SC315847; Origene) using fwd: 5′-ACA GTCGACATGTCGAAGGGCCCCGG-3′ and rev: 5′-TCACCGGTT CACGACTGGAGGGTGTGG-3′ and cloned into pBluescript II KS (–) using SalI and AgeI restriction enzyme sites. EcoRI and HindIII sites were appended to the ends of WTsiR and Mut.siR gene blocks, digested, and cloned into the pBluescript II KS (–) with full-length UNK. Full-length WTsiR and Mut.siR UNK from pBluescript II KS (–) were amplified and cloned into the lentivirus pCW57.1 N-term mCherry-BLAST construct for inducible doxycycline expression of pCW57.1-mCherry-WTsiR UNK and pCW57.1-mCherry-Mut.siR UNK. Sequencing of these constructs was confirmed using nanopore sequencing.

Generation of CRISPR *UNK* mut. cells

The pLenti-Crispr-V2 plasmid containing the gRNA sequence: 5′-GGCAGCCCGTCTAACCTCTG-3′ was used to target exon 13 of the *UNK* gene in RPE-1 *TP53* KO cells. Single cells were isolated by limiting dilution in a 96-well plate. Genomic DNA was isolated, and exon 13 was amplified using primers fwd: 5′-GAATTCTCA GCATTCTTCGTCAAAAG-3′ and rev: 5′-GAATTCCTGTCTTCA GCTGCAAATGG-3′. Sanger sequencing was used to confirm indel and premature stop codon formation.

Lentivirus transduction

Plasmids were isolated using ZymoPURE Plasmid Miniprep (D4208T). HEK293T cells at 60% confluency in 10-cm dishes were transfected with 1.5 µg of psPAX2 second-generation lentiviral packaging plasmid (12260; Addenge), 0.5 µg of pMD2.G envelope-expressing plasmid, and 2 µg of pCW57-mCherry-WTsiRUNK and pCW57-mCherry-Mut.siRUNK in Opti-MEM (31985070; Life Technologies), using the Lipofectamine 2000 Transfection Reagent (11668027; Thermo Fisher Scientific) according to the manufacturer's instructions. The following 2 days, medium containing viral particles was removed from HEK293T cells and added to RPE-1/Tet-PLK4 Cetn2-GFP with 10 µg/ml of polybrene. Transduced cells were selected with 10 µg/ml blasticidin for 1 wk prior to isolating clonal cell lines.

Immunofluorescence

Cells were fixed in cold MeOH for 8 min, washed three times in PBS, permeabilized with 0.5% Triton X-100 in PBS, and blocked in Knudsen buffer (1X PBS, 0.5% BSA, 0.5% NP-40, 1.0 mM $MgCl_2$, and 1.0 mM NaN_3) for 1 h. Cells stained for tubulin were fixed with glutaraldehyde and formaldehyde, as previously described (Canman et al., 2000). Briefly, cells were fixed with 4% paraformaldehyde and 0.5% glutaraldehyde in PIPES, HEPES, EGTA, and $MGSO_4$ (PHEM) and permeabilized in 0.5% Triton X-100 in PHEM. Coverslips were carefully quenched two times with sodium borohydride in PHEM for 5 min each time, followed by 3-, 5-min washes of 0.1% Triton X-100 PHEM and blocked with Knudsen buffer for 1 h.

Antibody staining was conducted at room temperature for 1–2 h. Samples were washed four times for 5 min each in PBS prior to secondary antibody and DNA staining in Knudson buffer for 1 h, except for samples stained for tubulin, in which fixation, staining, and washing were conducted in PHEM buffer. Primary antibodies: 1:1,000 rabbit α-UNK (HPA023636; Sigma-Aldrich), 1:1,000 rabbit α-STIL (a generous gift from J. Reiter, Department of Biochemistry and Biophysics, University of California, San Francisco School of Medicine, San Francisco, CA, USA), 1:1,000 rabbit α-CDK5RAP2 (50-157-1418; Bethyl), 1:1,000 rabbit α-PLK4 and 1:1,000 rabbit α-STIL (a generous gift from A. Holland, Department of Molecular Biology and Genetics, Johns Hopkins University School of Medicine, Baltimore, MD, USA), 1:5,000 guinea pig α-CEP131 (a generous gift from J. Reiter, Department of Biochemistry and Biophysics, University of California, San Francisco School of Medicine, San Francisco, CA, USA), 1:2,500 rabbit α-CEP152 (A302-480A; Bethyl), 1:2,000 goat α-CEP192 (a generous gift from A. Holland, Department of Molecular Biology and Genetics, Johns Hopkins University School of Medicine, Baltimore, MD, USA), 1:1,000 rabbit α-PCM1 (A301-150A; Bethyl), 1:1,000 rabbit α-CEP63 (16268-1-AP; Proteintech), 1:2,000 rabbit α-PCNT (ab4448; Abcam), and 1:1,000 mouse α-tubulin (CP06-100UG; Sigma-Aldrich). Secondary staining: 1:1,000 Alexa anti-rabbit 488 and 594, 1:1,000 Alexa anti-mouse 594, and 1:1,000 Alexa anti-guinea pig 594 and 647, and 1:1,000 Alexa anti-goat 594 (Thermo Fisher Scientific). Where appropriate, DNA was stained using Hoechst 33342 (62249; Thermo Fisher Scientific). Coverslips were mounted using Citifluor Af1 (17970-100; Electron Microscopy Services) and sealed with clear nail polish for confocal imaging and ProLong Gold Antifade (P10144; Thermo Fisher Scientific) for SIM.

Fluorescence imaging

Images were collected using a Yokogawa X1 spinning disk confocal on a Nikon Ti-E inverted microscope stand with a 100× Plan Apo NA 1.4 objective. Images were acquired at room temperature using 0.25-µm Z steps on an Andor iXon EM-CCD camera with exposure settings between 0 and 500 ms and 0 and 150 intensification, depending upon the experiment, and no binning of pixels using the SlideBook acquisition software. SIM images were acquired using a Nikon SIM on a Nikon Ti2 (LU-N3-SIM; Nikon Instruments) microscope equipped with a 100× SR Apo TIRF, NA 1.49 objective. Images were captured using a Hamamatsu ORCA-Flash 4.0 Digital CMOS camera (C13440) with 0.1–0.2-µm Z step sizes. Exposure settings were between 0 and 300 ms, depending upon the experiment. All images were collected at 25°C using NIS Elements software (Nikon). Raw SIM images were reconstructed using the image slice reconstruction algorithm (NIS Elements).

Centriole counts

GFP-centrin fluorescence was utilized to count centrioles manually using the 100× PlanApo DIC, NA 1.4 objective with a 1.5× magnification optivar on a Nikon TiE inverted microscope stand. Fields of view were randomly chosen.

Image analysis

Image analysis was performed using FIJI (Schindelin et al., 2012). Image stacks were projected by maximum intensity. Fluorescence intensities of centrosomes were measured within a 1-µm radius encompassing each individual centrosome. A measurement of cell intensity near each centrosome was acquired for non-centrosome signal background subtraction. To measure the fluorescence intensity of centriolar satellite proteins, fluorescence was measured within an 8.0-µm radius encompassing both centrosomes and the surrounding cytoplasm. The lowest intensity value found in the 8.0-µm radius was subtracted from the calculated radial intensities. If subtraction of background signal generated a negative fluorescence signal, it was converted to 0. For radial fluorescence intensity analyses, we utilized the Radial Profile Extended algorithm (ImageJ). Briefly, maximum intensity-projected images were selected for analysis. Centrosomes and cells identified by the algorithm were manually confirmed for accuracy prior to the algorithm calculating the in-cell radial fluorescence intensity.

To assess total fluorescence within a cell, background was subtracted from an average 5 × 5-µm box outside of the cell. The centrin channel was thresholded to generate a binary image encompassing the cell boundaries. This was subjected to the erode, dilate, and fill holes binary functions, followed by applying the create selection function. The selection was added to the region of interest manager and then transferred to the channel to be quantified.

Statistical methods and data collection

Centriole counts for two compared groups were analyzed using a t test with two tails. Fluorescence intensity measurements were compared using an unpaired *t* test with two tails. All statistics were calculated using Prism (GraphPad). Data distribution was assumed to be normal, but this was not formally tested. For multiple, or more than two comparisons, a one-way ANOVA with post hoc tests of Dunnett, Šidák, or Fisher's least significant difference was conducted where indicated. Investigators were not blinded when collecting data. Images were collected identically within experiments, and data analysis was automated to the extent possible to prevent bias.

smiFISH

Probes were generated using Stellaris probe design for the *UNK* gene and set to generate 48 probes. Probes were ordered from IDT. The reverse complement of the X FLAP sequence, 5′-CCT CCTAAGTTTCGAGCTGGACTCAGTG-3′, was added to the 5′ end of each probe. The 48 probes were resuspended to a final concentration of 100 µM and then combined to make a final equimolar probe mix of 100 µM. To create smiFISH duplexes, a 10 µl mixture consisting of a final concentration of 20 µM equimolar probe mix, 1x NEB3 buffer, and 25 µM Alexa Fluor 647-X FLAP (IDT) was combined. The duplexes were then assembled in a thermocycler with the following parameters: 85°C for 3 min, 65°C for 3 min, 25°C for 5 min, and then kept on ice or frozen at −20°C for storage. For RNA hybridization, cells were fixed onto 12-mm coverslips according to the LGC Biosearch Technologies RNA FISH protocol. Briefly, cells were fixed with 3.7% formaldehyde in PBS for 10 min, followed by one PBS wash. 70% ethanol was used for permeabilization at 4°C for 1 h. For each 12-mm coverslip, 1 µl of smiFISH duplexes in 50 µl of Stellaris RNA FISH Hybridization buffer (SMF-HB1-10; LGC Biosearch Technologies) was incubated on coverslips overnight at 37°C and washed with Stellaris RNA FISH Wash Buffer A (SMF-WA1-60; LGC Biosearch Technologies) three times for 5 min, followed by one final wash in Stellaris RNA Wash Buffer B (SMF-WB1-20; LGC Biosearch Technologies).

OPP labeling and click chemistry on fixed cells

Cells were labeled with OPP (NU-931-05; Jena Bioscience) at a final concentration of 50 µM in pre-warmed media for 15 min. Cells were then fixed in methanol for 8 min. Following fixation and three PBS washes, 500 µl total of click chemistry reagents at the final concentration of 10 mM Tris-Cl, pH 7.0, 0.1 mM CuSO4, 0.006 mM CY5 picolyl azide (1177-1; Vector Laboratories), 2 mM THPTA, 1 mM freshly made (+)-sodium L-ascorbate (1114-50G; Sigma-Aldrich Life Science), and DEPC-treated water were added per coverslip in a 24 well plate for 30 min at room temperature protected from light. Coverslips were washed three times with PBS for 5 min and either mounted or processed for antibody staining. For antibody staining, cells were permeabilized, blocked for 1 h, and incubated in primary antibody for 1 h, followed by three, 5-min washes in PBS. Secondary antibodies were incubated for 1 h, followed by three, 5-min washes in PBS. Cells were imaged on the same day. A decrease in OPP signal was observed following primary and secondary incubation overnight.

Western blot

For western blot, cells were lysed with whole cell lysis buffer (20 mM HEPES-KOH, pH 7.9, 10% glycerol, 300 mM KCl, 0.1% IGEPAL, 1 mM DTT, and 1X protease inhibitor cocktail [PI78440; Thermo Fisher Scientific]; 100 µl of lysis buffer per 1 × 10^6cells) by gentle inversion at 4°C for 30 min. After lysis, the tubes were spun at 17,000 × *g* for 30 min, and the supernatants were collected. The supernatants were mixed with an equal volume of lysis buffer without salt, producing a final salt concentration to 150 mM KCl. Total protein was quantified using the Quick Start Bradford Protein Assay (5000201; Bio-Rad). Approximately 30 µg of protein was mixed with 1x SDS loading buffer and boiled for 10 min. Western blots were blocked with TBS + 0.05% Tween-20 and 0.5% BSA for 1 h at room temperature and incubated in primary overnight in TBST + 0.5% BSA. After three TBST washes, blots were incubated in Licor IR680 or IR800 secondary antibodies at 1:20,000 for 1 h, washed three times with TBST, and imaged using a fluorescence Odyssey CLx Imager and LI-COR Acquisition Software (LICORbio).

RNA sequencing

RNA used for polyA-selected library generation for mRNA sequencing was isolated with the Monarch Total RNA Isolation Miniprep Kit (New England Biolabs). Libraries were constructed using the Nugen Universal Plus mRNA-SEQ library construction kit (0508; Nugen) and sequenced on an Illumina NovaSEQ 6000 sequencer by the Genomics and Microarray Shared Resource at the University of Colorado Cancer Center.

Bioinformatics

Bioinformatics was performed as previously described by Stemm-Wolf et al. (2021). Briefly, RNA-seq libraries were sequenced using an Illumina NovaSeq 6000 (2 × 150) to a depth of 60–100 million paired-end reads. Reads were trimmed using cutadapt (v1.16) to remove adapters and aligned to the hg38 genome using STAR v2.5.2a (Dobin et al., 2013). Gene counts were quantified using featureCounts v1.6.2 (Liao et al., 2013). Genes that were differentially regulated between endogenous and PLK4 overexpression were analyzed using DESeq2 v1.28.1 (Love et al., 2014).

Online supplemental material

Fig. S1 shows that the UNK mRNA and protein increased in PLK4-overexpressed cells; UNK's centrosome proximal localization; UNK RNAi depletion efficiency; generation of CRISPR *UNK* mut. cells; and PLK4, STIL, and CEP131 centrosomal levels in CRISPR *UNK* mut. cells. Fig. S2 shows the UNK depletion effect on the total cellular levels of PLK4, the localization and characterization of ectopic centrin puncta observed upon UNK loss, timing of PLK4-induced centriole overduplication, and the UNK depletion effect on PCM1 and CEP131 total cellular levels and localization to the centrosome. Fig. S3 shows the localization of mCherry UNK WTsiR and UNK mut.siR and their effects on centriole overduplication in PLK4-overexpressed cells, RNAi depletion efficiency of PCM1 and CEP131, the localization of CEP131 in UNK-depleted cells with expression of UNK WTsiR and UNK mut.siR, controls for OPP labeling and OPP levels at the

centrosome 6, 12, and 16 h after PLK4 overexpression, and the respective controls of GFP expression at these time points. The effect of cycloheximide treatment on PLK4-overexpressed cells, PCM1 and CEP131 Gene Ontology analysis, UNK depletion on whole cellular OPP levels, and OPP centrosomal levels upon UNK and CEP131 loss at 6 h after PLK4 overexpression are also shown. Data S1 shows the quantification of western blots in Fig. S1, B and F. Data S2 shows the quantification of western blots in Fig. S2, A and E.

Data availability

RNA sequencing data are available through Gene Expression Omnibus under accession number (GSE297133). Additional information regarding raw image files and data analyses are available upon request.

Acknowledgments

We are grateful to present and past Pearson lab members who provided insight and comments on the project. Jernej Murn (UC Riverside) provided reagents and helpful advice, Marisa Ruehle assisted with OPP and smiFISH experimental methods, and Andrew Holland (Johns Hopkins University) supplied the RPE-1 p53 KO cell line and antibodies. Jeremy Reiter (UC San Francisco) generously shared antibodies, and Meng-Fu Bryan Tsou (Sloan Kettering Cancer Center) supplied the RPE-1-Tet-PLK4 Cetn2-GFP p53 WT cell line.

This research was funded by the National Institutes of Health-National Institute of General Medical Sciences R35 GM140813 (C.G. Pearson), R35 GM140813 Diversity Supplement (A. Martinez), R35 GM133385 (J.M. Taliaferro), CU ASPIRE (J.M. Taliaferro and C.G. Pearson), and W.M. Keck Foundation (J.M. Taliaferro and C.G. Pearson).

Author contributions: A. Martinez: conceptualization, data curation, formal analysis, investigation, methodology, visualization, and writing—original draft, review, and editing. A.J. Stemm-Wolf: conceptualization, investigation, and writing—review and editing. R.M. Sheridan: formal analysis. J.M. Taliaferro: conceptualization, funding acquisition, and writing—review and editing. C.G. Pearson: conceptualization, funding acquisition, project administration, resources, supervision, validation, and writing—review and editing.

Disclosures: The authors declare no competing interests exist.

Submitted: 29 July 2024
Revised: 7 May 2025
Accepted: 26 June 2025

References

Arslanhan, M.D., D. Gulensoy, and E.N. Firat-Karalar. 2020. A proximity mapping journey into the biology of the mammalian centrosome/cilium complex. *Cells*. 9:1390. https://doi.org/10.3390/cells9061390

Aydin, Ö.Z., S.O. Taflan, C. Gurkaslar, and E.N. Firat-Karalar. 2020. Acute inhibition of centriolar satellite function and positioning reveals their functions at the primary cilium. *PLoS Biol.* 18:e3000679. https://doi.org/10.1371/journal.pbio.3000679

Bergalet, J., D. Patel, F. Legendre, C. Lapointe, L.P.B. Bouvrette, A. Chin, M. Blanchette, E. Kwon, and E. Lécuyer. 2020. Inter-dependent centrosomal co-localization of the cen and ik2 cis-natural antisense mRNAs in *Drosophila*. *Cell Rep.* 30:3339–3352.e6. https://doi.org/10.1016/j.celrep.2020.02.047

Bettencourt-Dias, M., A. Rodrigues-Martins, L. Carpenter, M. Riparbelli, L. Lehmann, M.K. Gatt, N. Carmo, F. Balloux, G. Callaini, and D.M. Glover. 2005. SAK/PLK4 is required for centriole duplication and flagella development. *Curr. Biol.* 15:2199–2207. https://doi.org/10.1016/j.cub.2005.11.042

Bhandari, D., T. Raisch, O. Weichenrieder, S. Jonas, and E. Izaurralde. 2014. Structural basis for the Nanos-mediated recruitment of the CCR4-NOT complex and translational repression. *Genes Dev.* 28:888–901. https://doi.org/10.1101/gad.237289.113

Brown, N.J., M. Marjanović, J. Lüders, T.H. Stracker, and V. Costanzo. 2013. Cep63 and cep152 cooperate to ensure centriole duplication. *PLoS One*. 8:e69986. https://doi.org/10.1371/journal.pone.0069986

Čajánek, L., T. Glatter, and E.A. Nigg. 2015. The E3 ubiquitin ligase Mib1 regulates Plk4 and centriole biogenesis. *J. Cell Sci.* 128:1674–1682. https://doi.org/10.1242/jcs.166496

Canman, J.C., D.B. Hoffman, and E.D. Salmon. 2000. The role of pre- and post-anaphase microtubules in the cytokinesis phase of the cell cycle. *Curr. Biol.* 10:611–614. https://doi.org/10.1016/s0960-9822(00)00490-5

Coelho, P.A., L. Bury, M.N. Shahbazi, K. Liakath-Ali, P.H. Tate, S. Wormald, C.J. Hindley, M. Huch, J. Archer, W.C. Skarnes, et al. 2015. Over-expression of Plk4 induces centrosome amplification, loss of primary cilia and associated tissue hyperplasia in the mouse. *Open Biol.* 5:150209. https://doi.org/10.1098/rsob.150209

Conkar, D., H. Bayraktar, and E.N. Firat-Karalar. 2019. Centrosomal and ciliary targeting of CCDC66 requires cooperative action of centriolar satellites, microtubules and molecular motors. *Sci. Rep.* 9:14250. https://doi.org/10.1038/s41598-019-50530-4

Cunha-Ferreira, I., I. Bento, A. Pimenta-Marques, S.C. Jana, M. Lince-Faria, P. Duarte, J. Borrego-Pinto, S. Gilberto, T. Amado, D. Brito, et al. 2013. Regulation of autophosphorylation controls PLK4 self-destruction and centriole number. *Curr. Biol.* 23:2245–2254. https://doi.org/10.1016/j.cub.2013.09.037

Dammermann, A., and A. Merdes. 2002. Assembly of centrosomal proteins and microtubule organization depends on PCM-1. *J. Cell Biol.* 159:255–266. https://doi.org/10.1083/jcb.200204023

Das, S., M. Vera, V. Gandin, R.H. Singer, and E. Tutucci. 2021. Intracellular mRNA transport and localized translation. *Nat. Rev. Mol. Cell Biol.* 22:483–504. https://doi.org/10.1038/s41580-021-00356-8

Debella, L.R., A. Hayashi, and L.S. Rose. 2006. LET-711, the *Caenorhabditis elegans* NOT1 ortholog, is required for spindle positioning and regulation of microtubule length in embryos. *Mol. Biol. Cell*. 17:4911–4924. https://doi.org/10.1091/mbc.e06-02-0107

Denu, R.A., M.M. Sass, J.M. Johnson, G.K. Potts, A. Choudhary, J.J. Coon, and M.E. Burkard. 2019. Polo-like kinase 4 maintains centriolar satellite integrity by phosphorylation of centrosomal protein 131 (CEP131). *J. Biol. Chem.* 294:6531–6549. https://doi.org/10.1074/jbc.RA118.004867

Denu, R.A., M. Shabbir, M. Nihal, C.K. Singh, B.J. Longley, M.E. Burkard, and N. Ahmad. 2018. Centriole overduplication is the predominant mechanism leading to centrosome amplification in Melanoma. *Mol. Cancer Res.* 16:517–527. https://doi.org/10.1158/1541-7786.MCR-17-0197

Dobin, A., C.A. Davis, F. Schlesinger, J. Drenkow, C. Zaleski, S. Jha, P. Batut, M. Chaisson, and T.R. Gingeras. 2013. STAR: Ultrafast universal RNA-seq aligner. *Bioinformatics*. 29:15–21. https://doi.org/10.1093/bioinformatics/bts635

Du, H., Y. Zhao, J. He, Y. Zhang, H. Xi, M. Liu, J. Ma, and L. Wu. 2016. YTHDF2 destabilizes m(6)A-containing RNA through direct recruitment of the CCR4-NOT deadenylase complex. *Nat. Commun.* 7:12626. https://doi.org/10.1038/ncomms12626

Duchaine, T.F., and M.R. Fabian. 2019. Mechanistic insights into MicroRNA-mediated gene silencing. *Cold Spring Harb. Perspect. Biol.* 11:a032771. https://doi.org/10.1101/cshperspect.a032771

Dzhindzhev, N.S., G. Tzolovsky, Z. Lipinszki, M. Abdelaziz, J. Debski, M. Dadlez, and D.M. Glover. 2017. Two-step phosphorylation of Ana2 by Plk4 is required for the sequential loading of Ana2 and Sas6 to initiate procentriole formation. *Open Biol.* 7:170247. https://doi.org/10.1098/rsob.170247

Enam, S.U., B. Zinshteyn, D.H. Goldman, M. Cassani, N.M. Livingston, G. Seydoux, and R. Green. 2020. Puromycin reactivity does not accurately localize translation at the subcellular level. *Elife*. 9:e60303. https://doi.org/10.7554/eLife.60303

Filippova, N., X. Yang, P. King, and L.B. Nabors. 2012. Phosphoregulation of the RNA-binding protein Hu antigen R (HuR) by Cdk5 affects centrosome function. *J. Biol. Chem.* 287:32277–32287. https://doi.org/10.1074/jbc.M112.353912

Ganapathi Sankaran, D., A.J. Stemm-Wolf, and C.G. Pearson. 2019. CEP135 isoform dysregulation promotes centrosome amplification in breast cancer cells. *Mol. Biol. Cell*. 30:1230–1244. https://doi.org/10.1091/mbc.E18-10-0674

Ghadimi, B.M., D.L. Sackett, M.J. Difilippantonio, E. Schröck, T. Neumann, A. Jauho, G. Auer, and T. Ried. 2000. Centrosome amplification and instability occurs exclusively in aneuploid, but not in diploid colorectal cancer cell lines, and correlates with numerical chromosomal aberrations. *Genes Chromosomes Cancer*. 27:183–190.

Gheiratmand, L., E. Coyaud, G.D. Gupta, E.M. Laurent, M. Hasegan, S.L. Prosser, J. Gonçalves, B. Raught, and L. Pelletier. 2019. Spatial and proteomic profiling reveals centrosome-independent features of centriolar satellites. *Embo J.* 38:e101109. https://doi.org/10.15252/embj.2018101109

Gillen, S.L., C. Giacomelli, K. Hodge, S. Zanivan, M. Bushell, and A. Wilczynska. 2021. Differential regulation of mRNA fate by the human Ccr4-Not complex is driven by coding sequence composition and mRNA localization. *Genome Biol.* 22:284. https://doi.org/10.1186/s13059-021-02494-w

Gupta, G.D., É. Coyaud, J. Gonçalves, B.A. Mojarad, Y. Liu, Q. Wu, L. Gheiratmand, D. Comartin, J.M. Tkach, S.W.T. Cheung, et al. 2015. A dynamic protein interaction landscape of the human centrosome-cilium interface. *Cell*. 163:1484–1499. https://doi.org/10.1016/j.cell.2015.10.065

Habedanck, R., Y.-D. Stierhof, C.J. Wilkinson, and E.A. Nigg. 2005. The Polo kinase Plk4 functions in centriole duplication. *Nat. Cell Biol.* 7:1140–1146. https://doi.org/10.1038/ncb1320

Hall, E.A., M. Keighren, M.J. Ford, T. Davey, A.P. Jarman, L.B. Smith, I.J. Jackson, and P. Mill. 2013. Acute versus chronic loss of mammalian Azi1/Cep131 results in distinct ciliary phenotypes. *PLoS Genet.* 9:e1003928. https://doi.org/10.1371/journal.pgen.1003928

Hall, E.A., D. Kumar, S.L. Prosser, P.L. Yeyati, V. Herranz-Pérez, J.M. García-Verdugo, L. Rose, L. Mckie, D.O. Dodd, P.A. Tennant, et al. 2023. Centriolar satellites expedite mother centriole remodeling to promote ciliogenesis. *Elife*. 12:e79299. https://doi.org/10.7554/eLife.79299

Hatch, E.M., A. Kulukian, A.J. Holland, D.W. Cleveland, and T. Stearns. 2010. Cep152 interacts with Plk4 and is required for centriole duplication. *J. Cell Biol.* 191:721–729. https://doi.org/10.1083/jcb.201006049

Hori, A., K. Barnouin, A.P. Snijders, and T. Toda. 2016. A non-canonical function of Plk4 in centriolar satellite integrity and ciliogenesis through PCM 1 phosphorylation. *EMBO Rep.* 17:326–337. https://doi.org/10.15252/embr.201541432

Ishigaki, Y., Y. Nakamura, T. Tatsuno, M. Hashimoto, K. Iwabuchi, and N. Tomosugi. 2014. RNA-binding protein RBM8A (Y14) and MAGOH localize to centrosome in human A549 cells. *Histochem. Cell Biol.* 141:101–109. https://doi.org/10.1007/s00418-013-1135-4

Jao, L.-E., A. Akef, and S.R. Wente. 2017. A role for Gle1, a regulator of DEAD-box RNA helicases, at centrosomes and basal bodies. *Mol. Biol. Cell*. 28:120–127. https://doi.org/10.1091/mbc.E16-09-0675

Jewett, C.E., B.L. Mccurdy, E.T. O'toole, A.J. Stemm-Wolf, K.S. Given, C.H. Lin, V. Olsen, W. Martin, L. Reinholdt, J.M. Espinosa, et al. 2023. Trisomy 21 induces pericentrosomal crowding delaying primary ciliogenesis and mouse cerebellar development. *Elife*. 12:e78202. https://doi.org/10.7554/eLife.78202

Kadyrova, L.Y., Y. Habara, T.H. Lee, and R.P. Wharton. 2007. Translational control of maternal Cyclin B mRNA by Nanos in the *Drosophila* germline. *Development*. 134:1519–1527. https://doi.org/10.1242/dev.002212

Kim, D.H., J.S. Ahn, H.J. Han, H.-M. Kim, J. Hwang, K.H. Lee, H. Cha-Molstad, I.-J. Ryoo, J.-H. Jang, S.-K. Ko, et al. 2019. Cep131 overexpression promotes centrosome amplification and colon cancer progression by regulating Plk4 stability. *Cell Death Dis.* 10:570. https://doi.org/10.1038/s41419-019-1778-8

Klebba, J.E., D.W. Buster, A.L. Nguyen, S. Swatkoski, M. Gucek, N.M. Rusan, and G.C. Rogers. 2013. Polo-like kinase 4 autodestructs by generating its Slimb-binding phosphodegron. *Curr. Biol.* 23:2255–2261. https://doi.org/10.1016/j.cub.2013.09.019

Kleylein-Sohn, J., J. Westendorf, M. Le Clech, R. Habedanck, Y.-D. Stierhof, and E.A. Nigg. 2007. Plk4-induced centriole biogenesis in human cells. *Dev. Cell*. 13:190–202. https://doi.org/10.1016/j.devcel.2007.07.002

Kodani, A., T.W. Yu, J.R. Johnson, D. Jayaraman, T.L. Johnson, L. Al-Gazali, L. Sztriha, J.N. Partlow, H. Kim, A.L. Krup, et al. 2015. Centriolar satellites assemble centrosomal microcephaly proteins to recruit CDK2 and promote centriole duplication. *Elife*. 4:e07519. https://doi.org/10.7554/eLife.07519

Kubo, A., H. Sasaki, A. Yuba-Kubo, S. Tsukita, and N. Shiina. 1999. Centriolar satellites: Molecular characterization, ATP-dependent movement toward centrioles and possible involvement in ciliogenesis. *J. Cell Biol.* 147:969–980. https://doi.org/10.1083/jcb.147.5.969

Kwon, O.S., R. Mishra, A. Safieddine, E. Coleno, Q. Alasseur, M. Faucourt, I. Barbosa, E. Bertrand, N. Spassky, and H. Le Hir. 2021. Exon junction complex dependent mRNA localization is linked to centrosome organization during ciliogenesis. *Nat. Commun.* 12:1351. https://doi.org/10.1038/s41467-021-21590-w

Lee, M., M.Y. Seo, J. Chang, D.S. Hwang, and K. Rhee. 2017. PLK4 phosphorylation of CP110 is required for efficient centriole assembly. *Cell Cycle*. 16:1225–1234. https://doi.org/10.1080/15384101.2017.1325555

Leppek, K., J. Schott, S. Reitter, F. Poetz, M.C. Hammond, and G. Stoecklin. 2013. Roquin promotes constitutive mRNA decay via a conserved class of stem-loop recognition motifs. *Cell*. 153:869–881. https://doi.org/10.1016/j.cell.2013.04.016

Lerit, D.A. 2022. Signed, sealed, and delivered: RNA localization and translation at centrosomes. *Mol. Biol. Cell*. 33:pe3. https://doi.org/10.1091/mbc.E21-03-0128

Levine, M.S., B. Bakker, B. Boeckx, J. Moyett, J. Lu, B. Vitre, D.C. Spierings, P.M. Lansdorp, D.W. Cleveland, D. Lambrechts, et al. 2017. Centrosome amplification is sufficient to promote spontaneous tumorigenesis in mammals. *Dev. Cell*. 40:313–322.e5. https://doi.org/10.1016/j.devcel.2016.12.022

Liao, Y., G.K. Smyth, and W. Shi. 2014. featureCounts: An efficient general purpose program for assigning sequence reads to genomic features. *Bioinformatics*. 30:923–930. https://doi.org/10.1093/bioinformatics/btt656

Liu, H., H. Li, Z. Jiang, S. Jin, R. Song, Y. Yang, J. Li, J. Huang, X. Zhang, X. Dong, et al. 2023. A local translation program regulates centriole amplification in the airway epithelium. *Sci. Rep.* 13:7090. https://doi.org/10.1038/s41598-023-34365-8

Love, M.I., W. Huber, and S. Anders. 2014. Moderated estimation of fold change and dispersion for RNA-seq data with DESeq2. *Genome Biol.* 15:550. https://doi.org/10.1186/s13059-014-0550-8

Marthiens, V., M.A. Rujano, C. Pennetier, S. Tessier, P. Paul-Gilloteaux, and R. Basto. 2013. Centrosome amplification causes microcephaly. *Nat. Cell Biol.* 15:731–740. https://doi.org/10.1038/ncb2746

Moyer, T.C., and A.J. Holland. 2019. PLK4 promotes centriole duplication by phosphorylating STIL to link the procentriole cartwheel to the microtubule wall. *Elife*. 8:e46054. https://doi.org/10.7554/eLife.46054

Murn, J., M. Teplova, K. Zarnack, Y. Shi, and D.J. Patel. 2016. Recognition of distinct RNA motifs by the clustered CCCH zinc fingers of neuronal protein Unkempt. *Nat. Struct. Mol. Biol.* 23:16–23. https://doi.org/10.1038/nsmb.3140

Murn, J., K. Zarnack, Y.J. Yang, O. Durak, E.A. Murphy, S. Cheloufi, D.M. Gonzalez, M. Teplova, T. Curk, J. Zuber, et al. 2015. Control of a neuronal morphology program by an RNA-binding zinc finger protein, Unkempt. *Genes Dev.* 29:501–512. https://doi.org/10.1101/gad.258483.115

Naslavsky, N., and S. Caplan. 2020. Endocytic membrane trafficking in the control of centrosome function. *Curr. Opin. Cell Biol.* 65:150–155. https://doi.org/10.1016/j.ceb.2020.01.009

Nigg, E.A., and A.J. Holland. 2018. Once and only once: Mechanisms of centriole duplication and their deregulation in disease. *Nat. Rev. Mol. Cell Biol.* 19:297–312. https://doi.org/10.1038/nrm.2017.127

Ohta, M., T. Ashikawa, Y. Nozaki, H. Kozuka-Hata, H. Goto, M. Inagaki, M. Oyama, and D. Kitagawa. 2014. Direct interaction of Plk4 with STIL ensures formation of a single procentriole per parental centriole. *Nat. Commun.* 5:5267. https://doi.org/10.1038/ncomms6267

Pascual, R., C. Segura-Morales, M. Omerzu, N. Bellora, E. Belloc, C.L. Castellazzi, O. Reina, E. Eyras, M.M. Maurice, A. Millanes-Romero, and R. Méndez. 2020. mRNA spindle localization and mitotic translational regulation by CPEB1 and CPEB4. *RNA*. 27:291–302. https://doi.org/10.1261/rna.077552.120

Peel, N., N.R. Stevens, R. Basto, and J.W. Raff. 2007. Overexpressing centriole-replication proteins in vivo induces centriole overduplication and de novo formation. *Curr. Biol.* 17:834–843. https://doi.org/10.1016/j.cub.2007.04.036

Pihan, G.A., A. Purohit, J. Wallace, H. Knecht, B. Woda, P. Quesenberry, and S.J. Doxsey. 1998. Centrosome defects and genetic instability in malignant tumors. *Cancer Res.* 58:3974–3985.

Rogers, G.C., N.M. Rusan, D.M. Roberts, M. Peifer, and S.L. Rogers. 2009. The SCF Slimb ubiquitin ligase regulates Plk4/Sak levels to block centriole

reduplication. *J. Cell Biol.* 184:225–239. https://doi.org/10.1083/jcb.200808049

Safieddine, A., E. Coleno, S. Salloum, A. Imbert, A.-M. Traboulsi, O.S. Kwon, F. Lionneton, V. Georget, M.C. Robert, T. Gostan, et al. 2021. A choreography of centrosomal mRNAs reveals a conserved localization mechanism involving active polysome transport. *Nat. Commun.* 12: 1352. https://doi.org/10.1038/s41467-021-21585-7

Schindelin, J., I. Arganda-Carreras, E. Frise, V. Kaynig, M. Longair, T. Pietzsch, S. Preibisch, C. Rueden, S. Saalfeld, B. Schmid, et al. 2012. Fiji: An open-source platform for biological-image analysis. *Nat. Methods*. 9: 676–682. https://doi.org/10.1038/nmeth.2019

Sepulveda, G., M. Antkowiak, I. Brust-Mascher, K. Mahe, T. Ou, N.M. Castro, L.N. Christensen, L. Cheung, X. Jiang, D. Yoon, et al. 2018. Co-translational protein targeting facilitates centrosomal recruitment of PCNT during centrosome maturation in vertebrates. *Elife*. 7:e34959. https://doi.org/10.7554/eLife.34959

Shah, K., S. He, D.J. Turner, J. Corbo, K. Rebbani, D. Dominguez, J.M. Bateman, S. Cheloufi, C. Igreja, E. Valkov, and J. Murn. 2024. Regulation by the RNA-binding protein Unkempt at its effector interface. *Nat. Commun.* 15:3159. https://doi.org/10.1038/s41467-024-47449-4

Singh, C.K., R.A. Denu, M. Nihal, M. Shabbir, D.R. Garvey, W. Huang, K.A. Iczkowski, and N. Ahmad. 2022. PLK4 is upregulated in prostate cancer and its inhibition reduces centrosome amplification and causes senescence. *Prostate*. 82:957–969. https://doi.org/10.1002/pros.24342

Sonnen, K.F., A.-M. Gabryjonczyk, E. Anselm, Y.-D. Stierhof, and E.A. Nigg. 2013. Human Cep192 and Cep152 cooperate in Plk4 recruitment and centriole duplication. *J. Cell Sci.* 126:3223–3233. https://doi.org/10.1242/jcs.129502

Staples, C.J., K.N. Myers, R.D.D. Beveridge, A.A. Patil, A.J.X. Lee, C. Swanton, M. Howell, S.J. Boulton, and S.J. Collis. 2012. The centriolar satellite protein Cep131 is important for genome stability. *J. Cell Sci.* 125: 4770–4779. https://doi.org/10.1242/jcs.104059

Staudacher, J., C. Rebnegger, and B. Gasser. 2021. Treatment with surfactants enables quantification of translational activity by O-propargyl-puromycin labelling in yeast. *BMC Microbiol.* 21:120. https://doi.org/10.1186/s12866-021-02185-3

Stemm-Wolf, A.J., E.T. O'toole, R.M. Sheridan, J.T. Morgan, and C.G. Pearson. 2021. The SON RNA splicing factor is required for intracellular trafficking structures that promote centriole assembly and ciliogenesis. *Mol. Biol. Cell*. 32:ar4. https://doi.org/10.1091/mbc.E21-06-0305

Tsherniak, A., F. Vazquez, P.G. Montgomery, B.A. Weir, G. Kryukov, G.S. Cowley, S. Gill, W.F. Harrington, S. Pantel, J.M. Krill-Burger, et al. 2017. Defining a cancer dependency map. *Cell*. 170:564–576.e16. https://doi.org/10.1016/j.cell.2017.06.010

Youn, J.-Y., W.H. Dunham, S.J. Hong, J.D.R. Knight, M. Bashkurov, G.I. Chen, H. Bagci, B. Rathod, G. Macleod, S.W.M. Eng, et al. 2018. High-density proximity mapping reveals the subcellular organization of mRNA-Associated granules and bodies. *Mol. Cell*. 69:517–532.e11. https://doi.org/10.1016/j.molcel.2017.12.020

Zhou, H., J. Kuang, L. Zhong, W.L. Kuo, J.W. Gray, A. Sahin, B.R. Brinkley, and S. Sen. 1998. Tumour amplified kinase STK15/BTAK induces centrosome amplification, aneuploidy and transformation. *Nat. Genet.* 20: 189–193. https://doi.org/10.1038/2496

JCB

Supplemental material

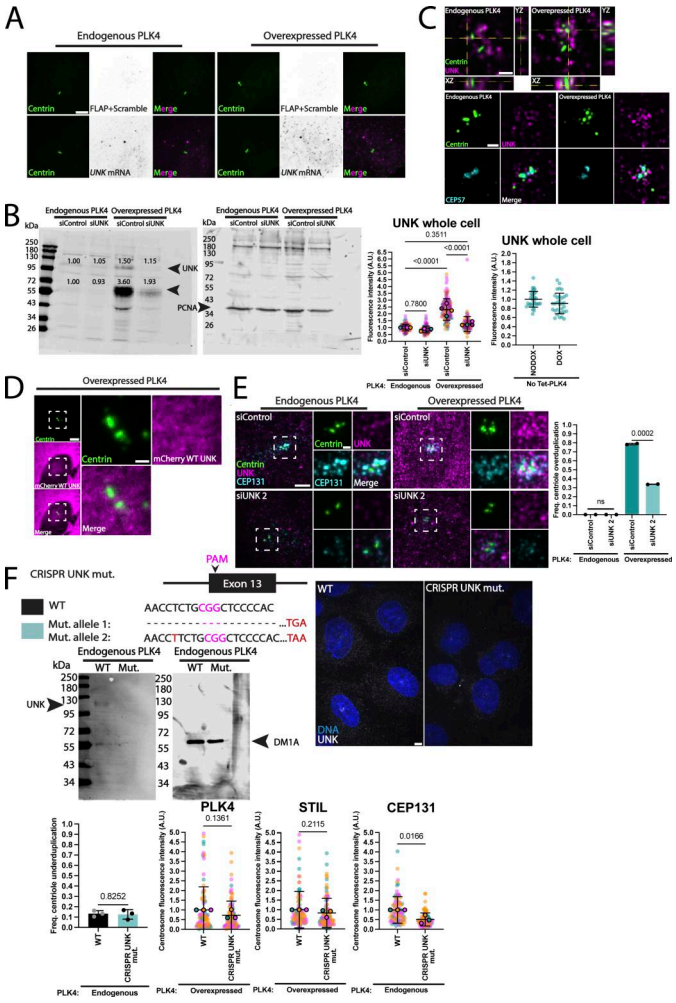

Figure S1. **The Unkempt RNA binding protein facilitates PLK4-induced centriole overduplication. (A)** PLK4 overexpression promotes elevated *UNK* mRNA levels. Confocal images of RPE-1-Tet-PLK4 Cetn2-GFP p53 WT cells showing *UNK* mRNA staining with endogenous and overexpressed PLK4 in S phase. *UNK* mRNA, grayscale, and centrioles (centrin), green. Scale bar, 5 µm. **(B)** siUNK #1 depletes whole-cell levels of UNK protein in RPE-1-Tet-PLK4 Cetn2-GFP p53 WT cells. Left—western blots of RPE-1-Tet-PLK4 Cetn2-GFP p53 WT cell lysates with UNK knockdown using siRNA #1 with endogenous and overexpressed PLK4 in S phase. Western blot stained with PCNA as a loading control and anti-UNK. Middle panel: Mean normalized fluorescence quantification of whole cell UNK protein levels with endogenous and overexpressed PLK4 in RPE-1-Tet-PLK4 Cetn2-GFP p53 WT cells. Graph values are expressed as means of four biological replicates of 25–30 cells per replicate and SD. P values were determined using one-way ANOVA with the Dunnett post hoc test. Right panel: Mean normalized fluorescence quantification of whole cell UNK protein levels with or without doxycycline in RPE-1 p53 KO cells. Graph values are expressed as means of biological one replicate of 25–30 cells and SD. **(C)** UNK localizes to the centrosomal region. Top panels: Z-projection from SIM images of endogenous UNK in RPE-1-Tet-PLK4 Cetn2-GFP p53 WT cells with endogenous and overexpressed PLK4 in S phase. UNK, magenta, and centrioles (centrin), green. Scale bar, 1 µm. Bottom panels: SIM images of endogenous UNK in RPE-1-Tet-PLK4 Cetn2-GFP p53 WT cells with endogenous and overexpressed PLK4. UNK, magenta; CEP57 (not equally scaled), cyan, and centrioles (centrin), green. Scale bar, 1 µm. **(D)** Exogenous expression of WTsiR UNK localizes to centrosomes. Confocal images of RPE-1-Tet-PLK4 Cetn2-GFP p53 WT cells showing expression of mCherry WT UNK at the centrosomes with PLK4 overexpression in S phase. UNK, magenta, and centrioles (centrin), green. Scale bar, 5 µm. Insets scale bar, 1 µm. **(E)** siUNK #2 depletes whole-cell levels of UNK protein in RPE-1-Tet-PLK4 Cetn2-GFP p53 WT cells and attenuates centriole overduplication. Left panels: Confocal images of RPE-1-Tet-PLK4 Cetn2-GFP p53 WT cells showing endogenous UNK protein in UNK-depleted cells with endogenous and PLK4 overexpression in S phase. UNK, magenta; CEP131, cyan; centrioles (centrin), green. Scale bar, 5 µm. Insets scale bar, 1 µm. Right panel: Frequency of cells with centriole overduplication. Graph values are expressed as the means of two biological replicates of 50 cells per replicate and SD. P value was determined using an unpaired two-tailed *t* test. **(F)** UNK is dispensable for canonical centriole duplication. Top left panels: CRISPR/cas9-mediated mutagenesis design in RPE-1 p53 KO cells for the *UNK* locus, showing CRISPR *UNK* mut. deletion and insertion leading to a premature stop codon in both alleles, respectively. Top right panels: Confocal images RPE-1 p53 KO CRISPR *UNK* mut. cells showing UNK antibody staining. UNK, grayscale, and DNA, blue. Scale bar, 5 µm. Middle panel: Western blots of RPE-1 p53 KO CRISPR *UNK* mut. cell lysates in S phase. Stained with DM1A as a loading control and anti UNK. Bottom left panel: Frequency of RPE-1 p53 KO UNK WT and CRISPR *UNK* mut. cells with centriole under duplication in S phase. Graph values are expressed as the means of three biological replicates of 50–75 cells per replicate and SD. P values were determined using an unpaired two-tailed *t* test. Bottom middle panels: Mean normalized centrosome fluorescence quantification of centrosomal PLK4 and STIL in RPE-1-Tet-PLK4 p53 KO UNK WT and CRISPR *UNK* mut. cells with overexpressed PLK4 in S phase. Graph values are expressed as the means of three biological replicates of 25–30 cells per replicate and SD. P values were determined using an unpaired two-tailed *t* test. Bottom right panel: Mean normalized centrosome fluorescence quantification of CEP131 binned central 2 µm in RPE-1p53 KO UNK WT and CRISPR *UNK* mut. cells in S phase. Graph values are expressed as the means of three biological replicates of 25–30 cells per replicate and SD. P values were determined using an unpaired two-tailed *t* test. Source data are available for this figure: SourceData FS1.

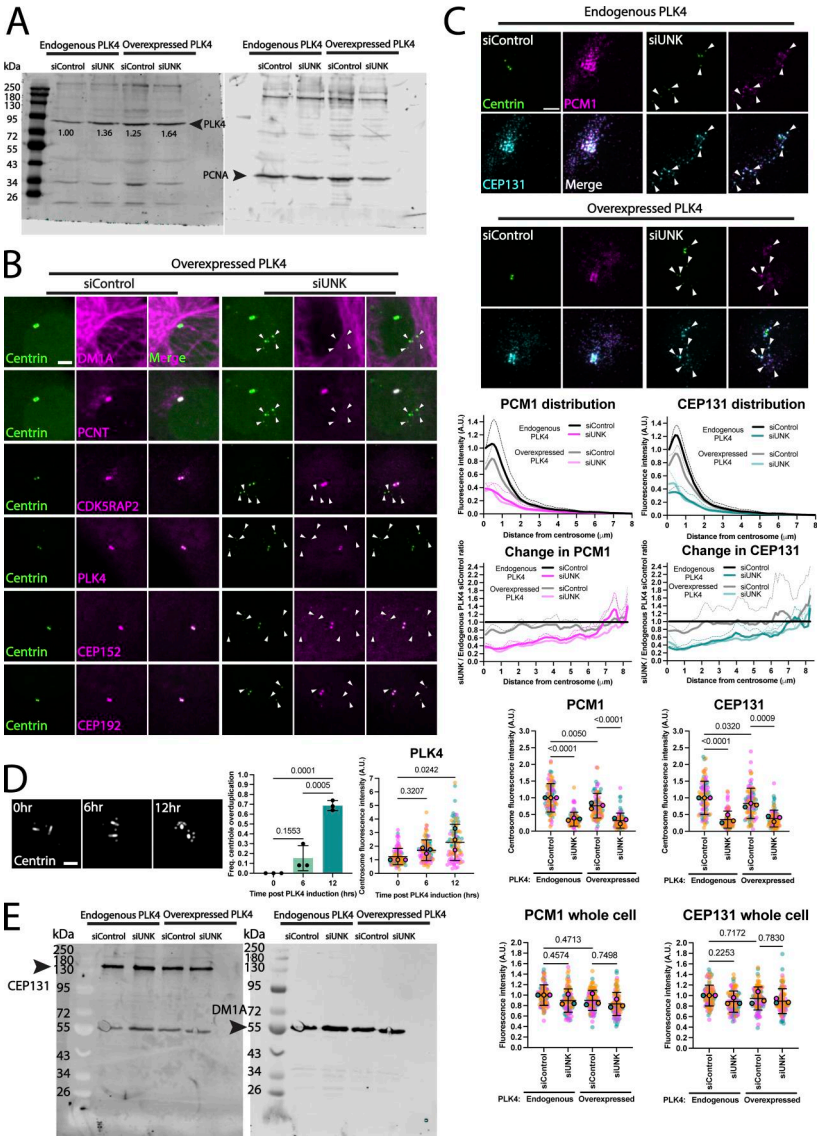

Figure S2. **UNK is a centriolar satellite protein and promotes PCM1 and CEP131 localization. (A)** Knockdown of UNK does not affect total cellular protein levels of PLK4. Western blot analysis of RPE-1-Tet-PLK4 Cetn2-GFP p53 WT cells depleted with siUNK #1. Cell lysates of RPE-1 cells with UNK knockdown using siRNA #1 with endogenous and overexpressed PLK4 in S phase. Western blot stained with PCNA from Fig. S1 B as a loading control, stripped, and re-probed with anti-PLK4. **(B)** UNK depletion results in ectopic centrin-positive foci that do not co-stain with MTs, PCM proteins, or centriole assembly proteins. Confocal images of RPE-1-Tet-PLK4 Cetn2-GFP p53 WT cells showing centrin-positive foci, green and stained for MTs (DM1A), PCM proteins (PCNT and CDK5RAP2), and centriole assembly proteins (PLK4, CEP152, and CEP192), magenta, in UNK-depleted cells with overexpressed PLK4 in S phase. Scale bar, 5 µm. Arrows indicate sites of no colocalization with ectopic centrin foci. **(C)** Centriolar satellites are reduced from the centrosome in UNK-depleted cells. Arrows indicate sites of colocalization with ectopic centrin foci. Insets scale bar, 5 µm. Top panels: Confocal images of RPE-1-Tet-PLK4 Cetn2-GFP p53 WT cells showing centriolar satellite localization in UNK-depleted cells with endogenous and overexpressed PLK4 in S phase. PCM1, magenta; CEP131, cyan; and centrioles (centrin), green. Scale bar, 5 µm. Middle top panels: 8.0-µm radial fluorescence intensity of PCM1 and CEP131 using centrin as the centrosome centroid. Middle bottom panels: 8 µm ratio quantification of PCM1 and CEP131 using centrin as the centroid. Bottom panels: Centrosomal PCM1 and CEP131 mean normalized fluorescence intensity based on binned central 2 µm. Graph values are expressed as the means of three biological replicates of 25–30 cells per replicate and SD. P values were determined using one-way ANOVA with the Šídák post hoc test. **(D)** Centriole overduplication occurs in a time-dependent manner after PLK4 overexpression. Left panels: SIM images of RPE-1-Tet-PLK4 Cetn2-GFP p53 WT cells showing centrioles 6 and 12 h after PLK4 overexpression in S phase. Centrioles (centrin), grayscale. Scale bar, 1 µm. Middle panel: Frequency of RPE-1-Tet-PLK4 Cetn2-GFP p53 WT cells with centriole overduplication 6 and 12 h after PLK4 overexpression in S phase. Graph values are expressed as the means of three biological replicates of 50 cells per replicate and SD. P values were determined using one-way ANOVA with the Šídák post hoc test. Right panel: Mean normalized centrosome fluorescence quantification of centrosomal PLK4 in RPE-1-Tet-PLK4 Cetn2-GFP p53 WT cells with centriole overduplication 6 and 12 h after PLK4 overexpression in S phase. Graph values are expressed as the means of three biological replicates of 25–30 cells per replicate and SD. P values were determined using one-way ANOVA with the Šídák post doc test. **(E)** Knockdown of UNK does not affect total cellular protein levels of CEP131. Left panels: Western blot analysis of RPE-1-Tet-PLK4 Cetn2-GFP p53 WT cells depleted with siUNK #1 with endogenous and overexpressed PLK4 in S phase. Western blot stained with DM1A, loading control, and anti PLK4. Right panels: Mean normalized fluorescence intensity of whole RPE-1-Tet-PLK4 Cetn2-GFP p53 WT cell PCM1 and CEP131 protein levels with endogenous and overexpressed PLK4 in S phase. Graph values are expressed as means of three biological replicates of 25–30 cells per replicate and SD. P values were determined using one-way ANOVA with the Šídák post hoc test. Source data are available for this figure: SourceData FS2.

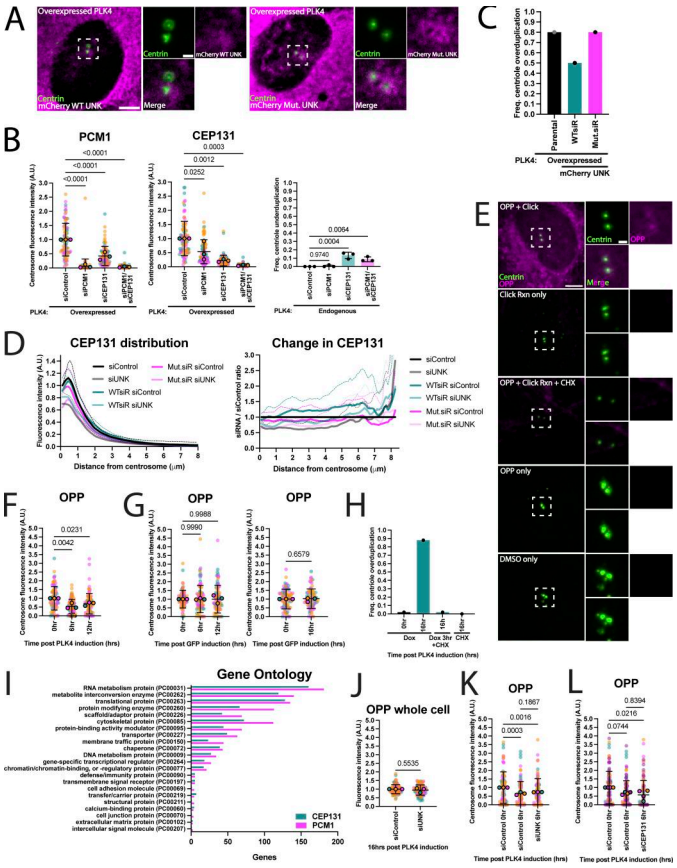

Figure S3. **UNK's RNA binding domain is required for PLK4-induced centriole overduplication. (A)** Exogenous expression of WTsiR and Mut.siR UNK localizes to centrosomes. Confocal images of RPE-1-Tet-PLK4 Cetn2-GFP p53 WT cells showing expression of mCherry WTsiR and Mut.siR UNK at the centrosomes with PLK4 overexpression in S phase. UNK, magenta, and centrioles (centrin), green. Scale bar, 5 µm. Insets scale bar, 1 µm. **(B)** Knockdown of PCM1 and CEP131 reduces centriolar satellites. Left panels: Centrosomal PCM1 and CEP131 mean normalized fluorescence intensities based on binned central 2 µm of RPE-1-Tet-PLK4 Cetn2-GFP p53 WT cells depleted with PCM1, CEP131, or double-depleted cells with overexpressed PLK4 in S phase. Graph values are expressed as the means of three replicates of 25–30 cells per replicate and SD. P values were determined using one-way ANOVA with the Dunnett post hoc test. Right panel: Frequency of centriole under duplication in RPE-1-Tet-PLK4 Cetn2-GFP p53 WT depleted with PCM1, CEP131, or double-depleted cells with endogenous PLK4 in S phase. Graph values are expressed as the means of three replicates of 100 cells per replicate and SD. P values were determined using one-way ANOVA with the Dunnett post hoc test. **(C)** High expression of WTsiR but not Mut.siR UNK blocks centriole overduplication. Frequency of RPE-1-Tet-PLK4 Cetn2-GFP p53 WT cells with PLK4 overexpression in S phase. Graph values are expressed as the mean of one biological replicate of 100 cells. **(D)** UNK's RNA-binding domain is dispensable for centriolar satellite localization. 8-µm radial fluorescence intensity and corresponding ratio quantification of CEP131 using centrin as the centrosome centroid of RPE-1-Tet-PLK4 Cetn2-GFP p53 WT cells with PLK4 overexpression in S phase. **(E)** OPP labels newly synthesized peptides and is blocked by cycloheximide. Confocal images of RPE-1-Tet-PLK4 Cetn2-GFP p53 WT cells with controls for OPP labeling: OPP with click chemistry fluor reaction, click chemistry fluor reaction without OPP, OPP with click chemistry fluor reaction with 50 µM of cycloheximide, OPP only, and DMSO only, all with PLK4 overexpression in S phase. OPP, magenta, and centrioles (centrin), green. Scale bar, 5 µm. Insets scale bar, 1 µm. **(F)** 6 and 12 h of PLK4 overexpression causes reduced translation at the centrosome. Mean normalized fluorescence quantification of centrosomal OPP levels 6 and 12 h of PLK4 overexpression in RPE-1-Tet-PLK4 Cetn2-GFP p53 WT cells in S phase. Graph values are expressed as means of three biological replicates of 25–30 cells per replicate and SD. P values were determined using one-way ANOVA with the Dunnett post hoc test. **(G)** 6, 12, and 16 h of GFP overexpression causes no effect of translation at the centrosome. Left panels: Mean normalized fluorescence quantification of centrosomal OPP levels 6 and 12 h of GFP overexpression in RPE-1-Tet-GFP p53 WT cells in S phase. Right panel: Mean normalized fluorescence quantification of centrosomal OPP levels with 16 h of GFP overexpression in RPE-1-Tet-GFP p53 WT cells in S phase. Graph values are expressed as means of three biological replicates of 25–30 cells per replicate and SD. P value was determined using a one-way ANOVA with the Dunnett post hoc test and unpaired two-tailed *t* test. **(H)** Further suppressing translation blocks centriole overduplication. RPE-1-Tet-PLK4 Cetn2-GFP p53 WT cells with PLK4 overexpression, followed by cycloheximide treatment, and frequency of centriole overduplication 16 h of PLK4 overexpression in S phase. Graph values are expressed as the mean of one biological replicate of 50 cells. **(I)** Centriolar satellites interact with proteins involved in RNA regulation. Panther analysis of BioID data from PCM1 and CEP131 interacting proteins (Gheiratmand et al., 2019) and their functional classification. **(J)** UNK does not impact translation on a whole-cell level 16 h of PLK4 overexpression. Mean normalized fluorescence quantification of whole-cell OPP levels with 16 h of PLK4 overexpression in RPE-1-Tet-PLK4 Cetn2-GFP p53 WT cells in S phase. Graph values are expressed as the means of three biological replicates of 25–30 cells per replicate and SD. P values were determined using an unpaired two-tailed *t* test. **(K)** UNK does not impact translation at the centrosome 6 or 12 h of PLK4 overexpression. Mean normalized fluorescence quantification of centrosomal OPP levels 6 and 12 h of PLK4 overexpression and depleted UNK in RPE-1-Tet-GFP p53 WT cells in S phase. Graph values are expressed as means of three biological replicates of 25–30 cells per replicate and SD. P values were determined using one-way ANOVA with the Šídák post hoc test. **(L)** CEP131 does not impact translation at the centrosome 6 or 12 h of PLK4 overexpression. Mean normalized fluorescence quantification of centrosomal OPP levels 6 and 12 h of PLK4 overexpression and depleted CEP131 in RPE-1-Tet-GFP p53 WT cells in S phase. Graph values are expressed as means of four biological replicates of 25–30 cells per replicate and SD. P values were determined using one-way ANOVA with the Šídák post hoc test.

Provided online are Data S1 and Data S2. Data S1 shows the quantification of western blots in Fig. S1, B and F. Data S2 shows the quantification of western blots in Fig. S2, A and E.